STADIUS
Center for Dynamical Systems, Signal Processing and Data Analytics

Citation/Reference	M. Lavanga et al., "Maturation of the autonomic nervous system in premature infants: estimating development based on heart-rate variability analysis," Front. Physiol. - Submiss., pp. 1–28, 2020.
Archived version	Author manuscript: the content is identical to the content of the published paper, but without the final typesetting by the publisher
Published version	Submitted
Journal homepage	https://www.frontiersin.org/journals/physiology
Author contact	your email mlavanga@esat.kuleuven.be your phone number +32 16 37 38 28
Abstract	This study aims at investigating the development of premature infants' autonomic nervous system (ANS) based on a quantitative analysis of the heart-rate variability (HRV) with a variety of novel features. Additionally, the role of heart-rate drops, known as bradycardias, has been studied in relationship to both clinical and novel sympathovagal indices. ECG data were measured for at least 3 hours in 25 preterm infants (gestational age ≤ 32 weeks) for a total number of 74 recordings. The postmenstrual age (PMA) of each patient was estimatedfrom the RR interval time-series by means of multivariate linear-mixed effects regression. The tachograms were segmented based on bradycardias in periods after, between and during bradycardias. For each of those epochs, a set of temporal, spectral and fractal indices were included in the regression model. The best performing model has R2 = 0.75 and mean absolute error MAE = 1.56 weeks. Three main novelties can be reported. First, the obtained maturation models based on HRV have comparable performance to other development models. Second, the selected features for age estimation show a predominance of power and fractal features in the very-low and low frequency bands in explaining the infants' sympathovagal development from 27 PMA weeks until 40 PMA 18 weeks. Third, bradycardias might disrupt the relationship between common temporal indices of the tachogram and the age of the infant and the interpretation of sympathovagal indices. This approach might provide a novel overview

	of postnatal autonomic maturation and an alternative development index to other electrophysiological data analysis.
IR	

(article begins on next page)

frontiers

Maturation of the autonomic nervous system in premature infants: estimating development based on heart-rate variability analysis

Mario Lavanga [1,*], **Elisabeth Heremans** [1], **Jonathan Moeyersons** [1], **Bieke Bollen** [2], **Katrien Jansen** [2], **Els Ortibus** [2], **Gunnar Naulaers** [2], **Sabine Van Huffel** [1], **Alexander Caicedo** [3]

[1] *Department of Electrical Engineering (ESAT), Division STADIUS, KU Leuven, Leuven, Belgium*
[2] *Department of Development and Regeneration, faculty of Medicine, KU Leuven, Belgium*
[3] *Applied Mathematics and Computer Science, School of Engineering, Science and Technology, Universidad del Rosario, Bogotá, Colombia*

Correspondence*:
Mario Lavanga
mlavanga@esat.kuleuven.be

ABSTRACT

This study aims at investigating the development of premature infants' autonomic nervous system (ANS) based on a quantitative analysis of the heart-rate variability (HRV) with a variety of novel features. Additionally, the role of heart-rate drops, known as bradycardias, has been studied in relationship to both clinical and novel sympathovagal indices. ECG data were measured for at least 3 hours in 25 preterm infants (gestational age ≤ 32 weeks) for a total number of 74 recordings. The postmenstrual age (PMA) of each patient was estimated from the RR interval time-series by means of multivariate linear-mixed effects regression. The tachograms were segmented based on bradycardias in periods after, between and during bradycardias. For each of those epochs, a set of temporal, spectral and fractal indices were included in the regression model. The best performing model has $R^2 = 0.75$ and mean absolute error $MAE = 1.56\ weeks$. Three main novelties can be reported. First, the obtained maturation models based on HRV have comparable performance to other development models. Second, the selected features for age estimation show a predominance of power and fractal features in the very-low and low frequency bands in explaining the infants' sympathovagal development from 27 PMA weeks until 40 PMA weeks. Third, bradycardias might disrupt the relationship between common temporal indices of the tachogram and the age of the infant and the interpretation of sympathovagal indices. This approach might provide a novel overview of postnatal autonomic maturation and an alternative development index to other electrophysiological data analysis.

Keywords: Preterm Infants, HRV, bradycardia, autonomic nervous system, maturation, development

1 INTRODUCTION

Premature infants represent 10% of the neonatal population and are at higher risk for development disorders that can lead to adverse outcome (Aylward, 2014). The investigation of maturation via multiple physiological biomarkers is part of the clinical practice to prevent lower cognitive, motor or language outcomes later on in life (Koolen et al., 2016), (Franke et al., 2012). A common probe to inspect the development of the neurovegetative functions or *Autonomic Nervous System* (ANS) is the heart-rate fluctuation, simply known as *Heart-rate variability* (HRV).

The guidelines of the adults HRV task force clearly specify the association between the different frequency tones of the tachograms and the stimulation of the ANS branches (Camm et al., 1996). The contribution of the sympathetic branch is represented by the low-frequency band (LF, $[0.04-0.15]$ Hz) of the HRV, while the high-frequency band (HF, $[0.15-0.5]$ Hz) reflects the parasympathetic branch. The sympathovagal balance can be expressed by the power ratio of the two frequency bands $\left(\frac{LF}{HF}\right)$, while the very-low frequency band (VLF, $[0-0.04]$ Hz) is usually associated to thermal and hormonal regulation. On the contrary, the fetal and preterm HRV frequency bands are still subject of an intensive discussion in the literature. The early exposure to the ex-utero environment induces an aberrant sympathetic response and delays autonomic maturation (Javorka et al., 2017),(Smith et al., 2013). The association between the common HRV frequency bands and the sympathovagal regulation is far less documented in infants and fetuses (Doret et al., 2015). Other factors are known to play a role in the definition of the oscillations of the heart-rate, such as intermittent breathing cycle with high respiratory frequency and the actual delay in maturation of the autonomic nervous system. Therefore, Doret et al. (Doret et al., 2015), David et al. (David et al., 2007) and Hoyer et al. (Hoyer et al., 2013) suggested that new ways to investigate the sympathovagal balance should be examined. Since the fetal heart-rate is characterized by a strong slow-wave baseline, David et al. redefine the frequency bands for fetuses as follows: $VLF = [0.02-0.08]$ Hz, $LF = [0.08-0.2]$ Hz, $HF = [0.2-3]$ Hz. While adults normally presents an HRV spectrum with two clear peaks at HF and LF (Camm et al., 1996), infants and fetuses have a $1/f$ spectrum up to 0.1 Hz (Karin et al., 1993). Consequently, the full description of the preterm ANS has to consider all the possible frequency bands (VLF,LF,HF) (Clairambault et al., 1992),(Longin et al., 2006),(Curzi-Dascalova, 1994),(Mazursky et al., 1998). This could explain why the $\frac{LF}{HF}$ ratio can give contradictory results: Krueger et al. (Krueger et al., 2010) did not find any specific change in this ratio in a longitudinal study with preterm patients, while Longin et al. (Longin et al., 2006) found a decrease in $\frac{LF}{HF}$ from preterm to term age. The rapid development and the unclear definition of the sympathovagal frequency bands might not give a simple interpretation of $\frac{LF}{HF}$ as it is for adults. Surprisingly, infants show bigger changes in the absolute power of the three main bands VLF, LF, and HF than relative power (Longin et al., 2006). Hoyer et al. (Hoyer et al., 2013) argued that predominant principles of autonomic development are not only an increase in heart-rate variability, but also increasing complexity and pattern formation. Consequently, HRV indices can be chosen to reflect these principles in order to describe the sympathovagal balance maturation. Pattern formation can be described by tachogram skewness and the new ratio $\frac{VLF}{LF}$, while the increasing complexity is characterized by an increasing HRV entropy. It should also be stressed that the computation of power ratios, such as $\frac{LF}{HF}$, requires stationarity, which can be questioned in case of infants heart-rate time series. Therefore, Abry et al. (Abry et al., 2010) and Doret et al. (Doret et al., 2015) proposed fractal analysis as an alternative method to to investigate the sympathovagal balance in fetal heart-rate. It

focuses on quantities such as oscillations or increments at different scales to tackle the absence of stationarity and determines a specific relations between the fractal exponents (such as the Hurst Exponent) and the $\frac{LF}{HF}$ ratios. However, those methods were never applied on premature infants.

One example of non-stationarity is the presence of bradycardias. These are normally heart-rate drops below 70% of the heart-rate average, which last at least for 4 s and may be associated with apneas. These drops can alter oxygen saturation and blood flow putting organs at risk of damage (Paolillo and Picone, 2013). In general, apneas and bradycardias can be uncorrelated, but apneic spells that occur with bradycardias are most likely to affect brain homeostasis. In addition, apneas and bradycardias are the probable consequence of the immature respiratory system, and the apneas' occurrence tends to decrease with increasing age (Atkinson and Fenton, 2009) (Porges, 1995). The bradycardia can then be considered a consequence of heart-rate disregulation, which can disrupt the state-space and the probability density function of the tachogram (Gee et al., 2017). Any proper model that tries to describe the development of the infants' ANS has to include not simply the slow variation of the basal heart-rate, but the sudden drops of the tachogram. Those nonstationary events possibly affect the most common HRV temporal or spectral features used in clinical practice and can bias conclusions of the medical community. For example, bradycardias can forcefully increase the variability of the tachogram or its regularity.

In order to address the shortcomings by the studies outlined above, a new framework to describe autonomic maturation in healthy preterm babies has been provided. This research can be divided in two main strands. First, both spectral analysis and multifractal analysis have been employed to investigate the neurovegetative development of the sympathovagal balance and its complexity and track maturation. Second, the impact of bradycardias on ANS maturation has been investigated. This study tries to provide a complete overview of autonomic maturation in premature neonates, including non-stationary events such as bradycardias. The final clinical objective is to provide novel maturation charts for the premature autonomic nervous system in the first weeks of life and correct the effect of heart-rate events on common clinical HRV indices. Those normative charts might be used as reference to investigate early-life and ex-utero factors that can deviate from a normal premature development and define suitable therapies in the neonatal intensive care unit.

2 METHODS

2.1 Dataset

The dataset consists of electrocardiograms (ECG) of 25 preterm infants, that were recorded at the Neonatal Intensive Care Unit of the University Hospital of Leuven. It was collected in a multimodal setting for another research study related to brain development and a sleep-stage analysis (Dereymaeker et al., 2017),(Koolen et al., 2016). Inclusion criteria were: a normal neurodevelopmental outcome at 9 and 24 months corrected age (Bayley Scales of Infant Development-II, mental and motor score > 85), no severe brain lesions, assessed by ultrasound, and not taking any sedative or antiepileptic drugs during the EEG registration. The sampling ECG frequency was 250 or 500 Hz and the average length of the recording was 4h 44 min. An overview of the dataset is reported in Table 1, while a complete description is reported in Table S1 and S2. The latter show the heterogenous interperiod sessions among recordings, which indicate that the measurements were

not scheduled at the same PMA for each patient. In addition, the supplementary materials S1 ad S2 show the ECG sampling frequency for each of the recording.

Table 1. Demographics of the 25 patients: average duration of the tachogram in minutes (Duration_{Rec}), average duration of the annotated bradycardias in s (Duration_{WB}),average number of the annotated bradycardias (Number_{WB}), average RR amplitude during the bradycardia in ms (RR_{WB}), postmenstrual age in weeks (PMA) and gestational age in weeks (GA). The last three rows represent the number of recording for each age subgroup (below 32 PMA weeks, between 32 and 36 weeks and above 36 weeks).

Number of patients = 25	
Duration_{Rec} (min)	208.435 ± 115.657
Duration_{WB} (s)	18.881 ± 8.332
Number_{WB}	7 ± 12
RR_{WB}	631.405 ± 78.677
PMA (wks)	33.689 ± 3.049
GA (wks)	28.315 ± 2.318
$PMA \leq 32\ wks$	22
$PMA \in (32-36]\ wks$	35
$PMA > 36\ wks$	17

2.2 Preprocessing

The HRV represents the instantaneous fluctuations of heart rate and is usually expressed by the tachogram which visualizes the variations of the time interval between two consecutive R-peaks (RR intervals, RR_i). In order to compute a RR_i time series, the R peaks of the ECG have been detected via the Matlab toolbox by Moeyersons et al. (Moeyersons et al., 2019), which is based on enveloping procedure. This graphical user-interface also allows for correction and deletion in case of erroneous R-peaks. In case of a single missing R-peak, the value was replaced by using the formula:

$$\hat{R}_t = \frac{R_{t-1} + R_{t+1}}{2}, \tag{1}$$

where $\hat{R}_t$ is the estimated position of the missed R-peak, while R_{t-1} and R_{t+1} are the location of the previous and following R-peak. In case of two or more missing R-peaks due to ECG flat lines or muscle artifacts which made the QRS detection impossible, the contaminated parts of the signal were discarded. In case that less 20 minutes of noise-free signal remained, the signal was discarded. The length of each recording (in min) is reported in in Table S1 and S2. The progressive number of the recording ID shows that some of them were fully discarded. The full overview shows that all included recordings had at least 50 minutes of available data (Duration_{Rec} column) resulting in a total of 74 recordings.

Besides the preprocessing of artifacts and before the feature extraction, we also dealt with the sudden drops of heart-rate, known as bradycardias. Although those phenomena are completely natural in the developing infant, they can suddenly increase the frequency content of the RR_i series. Therefore, traditional linear spectral and temporal analysis might not be suitable since the

instantaneous variance and mean of the heart-rate can vary over time, as explained in detail by (Gee et al., 2017). According to the same study, the heart-rate activity that precedes sudden drops might differ from the drops itself and other bradycardia-free periods. Consequently, bradycardias have been detected in the current studies before any further processing. Based on the definitions of apnea of prematurity and bradycardias by (Paolillo and Picone, 2013), the bradycardia spells were detected as sudden RR_i increases above 1.5*$\overline{RR_i}$ that persist for more than 4 s, where $\overline{RR_i}$ is the median tachogram of the entire recording. Subsequently, three different windowing strategies were applied:

1. Post-bradycardia (PB) windowing: the immediate 10 minutes after the bradycardic event were considered a candidate for features' extraction. It is important to remember this window did not include the bradycardia itself.
2. Between-bradycardias (BB) windowing: all non-overlapping 10 minute windows contained between bradycardic events were considered as candidate epochs for features' extraction. The first viable window was at least 10 minutes away from the bradycardic event in order to guarantee that the signal was stabilized.
3. Within-bradycardia (WB) windowing: a 10 minute window was considered from the moment that the signal exceeds the threshold 1.5*$\overline{RR_i}$ in the tachogram, i.e. the supposed start of the bradycardic event. This windowing should involve both the information related to the heart-rate drop and the recovery period.

A visual description of the windowing scheme is reported in Figure 1. The grey dashed boxes highlight the three type of windows (WB,BB,PB) that can be determined in a single trace, while the dot-dash box shows typical bradycardia events.The average duration and amplitude of a bradycardia event is reported in Table 1, which also shows the average number of bradycardias in the entire dataset. A full overview recording by recording is reported in the supplementary Table S1 and S2, which display the number of bradycardias as well as the average intensity and the average duration of heart-rate drops patient by patient. The supplementary materials show that some of the recordings did not have any heart-rate drop according to the reported definition. Therefore, the windowing scheme based on bradycardias was not applicable. In this specific case, the design choice was a segmentation in non-overlapping 10 minutes windows and assign the results of feature extraction to post-bradycardia windowing scheme (see Figure 2).

2.3 Feature extraction

In each of the windows defined according to the PB,BB and WB schemes, a set of temporal, spectral and fractal features were derived to describe the autonomic nervous system of the premature infants and its relationship with development. An overview of the different attributes is reported in Table 2.

2.3.1 Temporal Indices

Based on the most common guidelines related to HRV processing (Javorka et al., 2017) and (Camm et al., 1996), the first and the second order moments of the RR_i, i.e. the mean of the tachogram (μ_{RR}) and the standard deviation (σ_{RR}), were computed in order to assess the level of the variability.

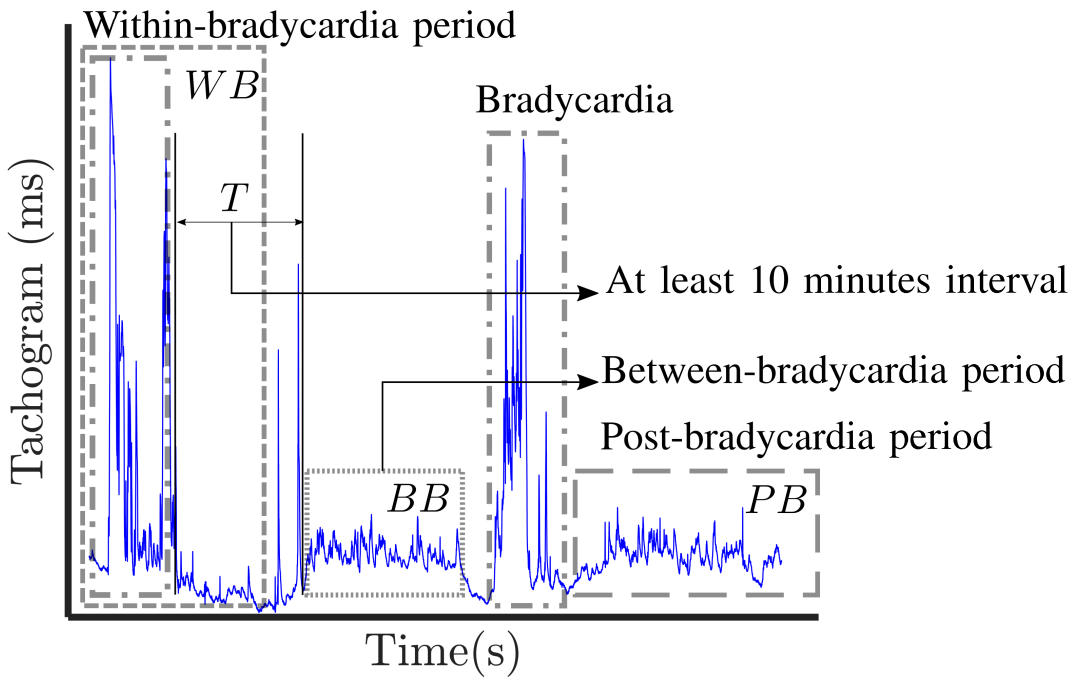


Figure 1. Visual representation of the three windowing schemes applied in this study: postbradycardia scheme (PB), between-bradycardia scheme (BB) and within-bradycardia scheme (WB). The selected windows in each trace are indicated with grey dashed boxes, while the dot-dashed boxes show examples of annotated bradycardia. In case of BB windowing, a period T greater that 10 minutes is present between the end of the bradycardia and the first available window.

2.3.2 Spectral analysis

The sympathovagal activity is normally assessed by the computation of the spectral power in the different HRV frequency bands (Camm et al., 1996). Unlike adults, the premature infants have a higher mean heart-rate with very slow oscillation around it (David et al., 2007),(Clairambault et al., 1992). Therefore, the frequency bands of the premature patients were defined as follows: $VLF = [0, 0.08]\ Hz$, the low-frequency $LF = [0.08, 0.2]\ Hz$ and high frequency $HF = [0.2, 3.0]\ Hz$. Additionally, the RR time series of the premature infant can be nonstationary due to a series of events, like bradycardias or other heart-rate disregulation. Therefore, the power spectral density was computed with time-frequency (TF) methodologies. Namely, the HRV power spectral density (PSD) was estimated with three specific approaches: the Welch's periodogram, the quadratic smoothed pseudo Wigner-Ville distribution (SPWD) (Orini et al., 2012) and the continuous wavelet transform (CWT) (David et al., 2007).

Given a fixed window size, Welch's algorithm estimates multiple periodograms in overlapping subwindows and averages them. The Welch's window length was set at 3 minutes and the overlap at 50%. Based on the suggestions of the HRV guidelines (Camm et al., 1996), the window length was set to investigate the very-low frequency band.

One can also estimate the instantaneous autospectrum $S_{RR}(t, f)$. Based on the CWT of the tachogram

$$W_{RR}(t,s) = \int_{-\infty}^{+\infty} RR(\tau)\psi^*\left(\frac{t-\tau}{s}\right)d\tau, \tag{2}$$

$S_{RR}(t,f)$ can be computed as the scalogram of the wavelet transform of the signal as follows:

$$S_{RR}(t,f) = |W_{RR}(t,f)|^2, \tag{3}$$

where ψ is the mother wavelet (Analytic Morlet), while s stands for the scale of the wavelet transform and, in the general, $s \approx f^{-1}$. However, the $S_{RR}(t,f)$ based on CWT risks to be distorted by interference terms which can be present with linear time-frequency approaches. Therefore, Orini (Orini et al., 2012) proposed to estimate the instantaneous autospectrum via a quadratic time-frequency distribution, such as SPWD. Then S_{RR} is then estimated as follows:

$$S_{RR}(t,f) = \int\int_{-\infty}^{+\infty} \Phi_{RR}(\tau,\nu)A_{RR}(\tau,\nu)e^{j2\pi(t\nu-\tau f)}d\tau d\nu, \tag{4}$$

where $A_{RR}(\tau,\nu)$ is the ambiguity function, which is defined as the Fourier Transform of the time-dependent auto-correlation of $RR(t)$ as follows

$$A_{RR}(\tau,\nu) = \int_{-\infty}^{+\infty} RR(t+\tau/2)RR^*(t-\tau/2)e^{-j2\pi t\nu}dt, \tag{5}$$

The smoothing of the time-frequency cross-coupling in (4) is done via the exponential kernel in the ambiguity domain defined as

$$\Phi_{RR}(\tau,\nu) = \exp\left\{-\pi\left[\left(\frac{\nu}{\nu_0}\right)^2 + \left(\frac{\tau}{\tau_0}\right)^2\right]^{2\lambda}\right\}, \tag{6}$$

Following the study by (Widjaja et al., 2013), ν_0, τ_0, λ were set to 0.050, 0.046, and 0.3, respectively, leading to a kernel function with a TF resolution of [Δt, Δf] = [10.9 s, 0.03 Hz]. Both Welch's approach and the CWT were computed with MATLAB subroutines, while the implementation details and software download for the SPWD are reported in (Orini et al., 2012).

Based on the given methodologies, the instantaneous power in the $\beta = [f_1, f_2]$ band of interest can be obtained as

$$P_\beta(t) = \int_{f1}^{f2} S_{RR}(t,f)df. \tag{7}$$

In particular, one can compute the absolute power in three bands VLF, LF and HF as the reported integral in (7). Besides, the ratios $\frac{VLF}{LF}$ and $\frac{LF}{HF}$ were also computed alongside two indices to represent the normalized LF power: $\frac{LF}{VLF+LF}$ and $\frac{LF}{HF+LF}$. In case of Welch's algorithm, there is no dependency from the time variable t. On the contrary, CWT and SPWD generates a time series for each selected frequency band, as highlighted by (4),(3) and (7). In order to obtain one single

value for each window, the median of this time-series was taken into account. The set of spectral features derived for each methodology is reported in the central block of Table 2.

2.3.3 Multifractal analysis

Since spectral analysis requires stationarity of data and the very definition of the tachogram series frequency bands have been questioned, the HRV was also analyzed according to the fractal or multifractal paradigm. As shown in (Doret et al., 2015), the infant's tachogram is a fractal or scale free signal, which presents a power-law decay spectrum as follows:

$$S_{RR}(f) = |C| f^{-2(H_{exp}-1)} \tag{8}$$

where H_{exp} is known as the Hurst exponent and controls the decay of the power function. H is also a representative parameter for fractal time series and there can be more than one exponent for each signal. A signal with one single exponent is commonly known as monofractal, while a signal with multiple exponents h is known as multifractal (Ivanov et al., 1999). Small values of h represent sharp and transient regularity or singularity, while large values represent smooth changes (Leonarduzzi et al., 2010).

An efficient method to determine the amount of exponents or singularities h is the multifractal formalism based on the wavelet transform modulus maxima. The discrete wavelet transform (DWT) decomposes the signal $RR(t)$ into elementary time-frequency components based on different scales a. Large scales describe smooth and low frequency oscillations, while small scales describe the sharp transitions in the signal. According to (Wendt et al., 2007) and (Popivanov et al., 2006), a partition function $Z(a,q) = Z_L(2^j, q)$ can be estimated using the *wavelet leader* $L_f(j,k)$, as follows:

$$Z(a,q) = Z_L(2^j, q) = \frac{1}{n_k} \sum_{k=1}^{n_k} |L_f(j,k)|^q \sim 2^{j\tau(q)}, \tag{9}$$

where $L_f(j,k)$ represents a specific type of wavelet transform, where the maximum of wavelet coefficients is considered in a narrow time neighborhood. More details can be found in (Abry et al., 2010),(Wendt et al., 2007).

One can immediately notice the similarity between (8) and (9), especially between the Hurst exponents and $\tau(q)$. For certain values of q, the scaling exponent $\tau(q)$ (SE) has a specific meaning: for positive respectively negative q, $Z(a,q)$ reflects scaling of large respectively short fluctuations. In general, for each q, the partition function exhibits a power-law decay characteristic, such as the power spectrum of $1/f$ noise (8). The scaling exponents $\tau(q)$ (SE) associated to this decay can be obtained by computing the slope of Z versus the scales in a log-log diagram from a certain scale $a_1 = 2^{j_1}$ to a certain scale $a_2 = 2^{j_2}$. The log-transform clearly shows the advantage to define scales as power quantities. In case of a monofractal signal, $\tau(q)$ is a linear function of q and H_{exp}, which is $\tau(q) = qH_{exp} - 1$ (as also shown in (8)). In case of a multifractal signal, the $\tau(q)$ is a nonlinear function of the local exponents h and its fractal dimensions $D(h)$, known also as singularity spectrum (SS) (Popivanov et al., 2006).

The fractal paradigm fully describes the properties of the signal by means of the singularity spectrum $D(h)$, obtained as the Legendre transform of $\tau(q)$ (Abry et al., 2010). This function represents the embedding dimensions in function of the different singularities of the signals and two main $D(h)$ attributes are normally derived: the maximum and the width of the $D(h)$ distribution, known also as the parameters C_1 and C_2. They can be computed as cumulants or coefficients of the Taylor expansion of $\tau(q)$ and they are used to represent the main Hurst exponent of the multifractal signal (H_{exp} or C_1) and the "variety" of fractals in the time series (C_2).

The multifractality parameters (H_{exp}, C_2) were computed in the entire non-overlapping window according to three schemes discussed in Section 2.2. Specifically, the multifractal features were derived using the Wavelet p-Leader and Bootstrap based MultiFractal analysis (PLBMF) MATLAB toolbox, described in Wendt et al. (2007). This toolbox can be downloaded from `https://www.irit.fr/~Herwig.Wendt/software.html`. A fundamental design choice is the scale range $[2^{j_1}, 2^{j_2}]$ from which the exponent $\tau(q)$ is estimated from (9) (Abry et al., 2010), (Wendt et al., 2007). In case of HRV, the exponents $[j_1, j_2]$ are normally set equal to $[3, 12]$. Given the fact that the scale can be written as $a = 2^j = (f_s/2)/f$ with f_s as sampling frequency of the signal, it follows that the range $[j_1, j_2] = [3, 12]$ approximately represents the frequency band $\approx [0.375, 0.001]\ Hz$ with $f_s = 6\ Hz$. In case that $[j_1, j_2] = [5, 12]$, the chosen scale range approximately represents the frequency band $\approx [0.094, 0.001]\ Hz$. It is clear the first range considers part of the HF band, while the latter solely focuses on the combination of LF and VLF. Since the chosen scale range might influence the multifractal attributes, both ranges were tested in this study to investigate which frequency bands mostly reflects the sympathovagal balance. In fact, the main Hurst exponent H_{exp} or C_1 parameter is able to influence the ratio $\frac{LF}{HF}$. Based on (8), one can rewrite the spectral ratios as:

$$\frac{LF}{HF} = \frac{\int_{f_m}^{f_I} S_{RR}(f)df}{\int_{f_I}^{f_M} S_{RR}(f)df} = \frac{(f_I^{2-2H_{exp}} - f_m^{2-2H_{exp}})}{(f_M^{2-2H_{exp}} - f_I^{2-2H_{exp}})} \tag{10}$$

where $[f_m, f_I]$,$[f_I, f_M]$ represent the frequency bands of LF and HF. Taking into account that the Hurst exponent and the $\frac{LF}{HF}$ are related and taking also into account that the chosen $[j_1, j_2]$ decides which frequency bands the multifractal parameters are related to, the scales investigation of the fractal properties can shed a light which bands mainly reflect the sympathovagal activity. The set of fractal features derived for each methodology is reported in last block of Table 2.

2.3.4 Algorithmic pipeline and statistical analysis

The processing pipeline of the current study is reported in Figure 2. For each HR time series, the signal was split according to the PB,BB and WB windowing scheme reported in Figure 1 and all the features reported in Table 2 were extracted. Besides artifact removal, a fundamental preprocessing step is the resampling of the tachogram. The behavior of nonlinear features can depend on the sample rate, as also shown by the definition of the scales and their range for the multifractal parameters (Section 2.3.3). Based on the findings by (Bolea et al., 2016), the following sampling frequencies were tested for fractal indices: $[6, 8, 12]\ Hz$. In contrast, the sampling frequencies for

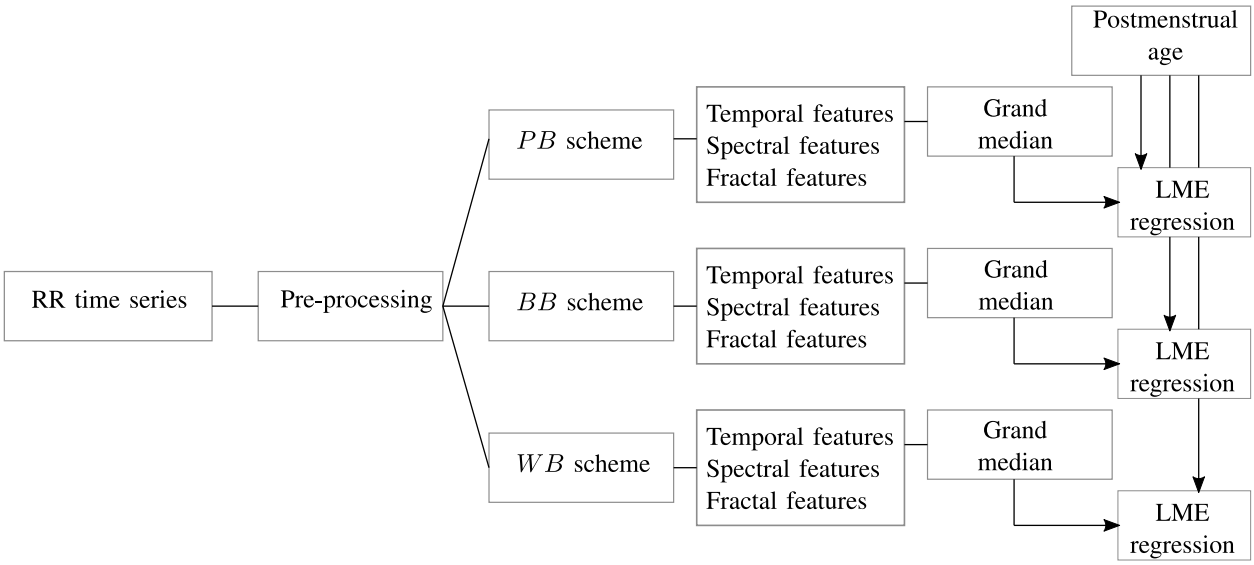


Figure 2. The block diagram shows the main steps of the study. For each RR signal, artifact preprocessing is performed and associated resampling of the tachogram. The signal is split in different windows according to the scheme of Figure 1. For each of these epochs, temporal, spectral and fractal features, which undergo a grand-median process if there is more than one epoch per scheme. The three datasets are then used to estimate the age of the recording in a linear mixed effects (LME) regression.

the spectral and temporal indices was set to $6\ Hz$ in order to include the higher respiratory frequency of premature infants (Camm et al., 1996),(Javorka et al., 2017).

As described in Section 2.3, the tuning and designed parameters for the spectral and fractal analysis were chosen in accordance to the absence of stationarity and the persistent slow-wave baseline of the premature HRV signal. The necessity to investigate long-range fluctuations and a recovery period after events such as bradycardias justify the segmentation in 10 minutes. Normally, time-frequency approaches use windows longer than 600 s to describe evolution in HRV spectrum (Widjaja et al., 2013),(Orini et al., 2012) and the fractal indices also requires windows of this size to fully investigate changes in regularity (Abry et al., 2010),(Doret et al., 2015). Additionally, the BB and WB schemes can generate a set of windows and therefore an array of features based on the number of bradycardias present in each recording (on average, 7 bradycardias per recording, as reported by Table 1). In order to obtain one representative value for each recording in each windowing scheme, the median of this array of attributes over the different windows was computed for each recording, as highlighted by the grand-median block in Figure 2.

After the features' extraction process and the grand-median step, three datasets were then obtained according to the three different windowing schemes. The number of features extracted for each dataset was then 27 in total: 21 for the spectral attributes, 2 for the temporal ones, 4 for fractal indices, as shown in Table 2.

In order to investigate the ANS maturation, the HRV features were used to estimate the PMA of the patient, as shown by the last block of the diagram in Figure 2. Since the PMA is known for each recording, a linear mixed effects (LME) regression model was developed for each dataset with PMA

as response variable (Lavanga et al., 2018). The actual regression consisted of two steps. First, the features were selected via the least absolute shrinkage and selection operator (LASSO) due to the high number of features, after that the absolute power features were log-transformed. Specifically, the LASSO was repeated for 20 iterations on the entire dataset and the features which were selected in more than 40% of the total number of iterations (8 iterations out of 20) were included in the regression model (Lavanga et al., 2018). Second, a linear mixed-effect regression model was built with the selected subsets with multiple random splits of the data. In particular, the dataset was split into 70% training set and 30% test set for 20 iterations and the model was developed on the train set and tested for test set for each iteration. The performance was then assessed as *mean absolute error* MAE on the test set, as well as explained variance R^2, both on train and test set (R^2_{train}, R^2_{test}). The results were reported as median(IQR) (where IQR stands for *InterQuartile Range*) over the 20 iterations. A linear-mixed effect model requires the definition of a grouping variable which introduces the random effect and the patient ID was taken as grouping variable since a set of one or more recordings belong to a patient (as discussed in a previous study (Lavanga et al., 2018)) . Furthermore, the LME regression with the LASSO procedure was not simply examined for the entire subset of features, but also for the three subset feature groups: temporal, spectral and fractal attributes. In case of temporal features regression, the LASSO step was not performed.

On top of that, the trend for the ANS features throughout the patients' development was also reported as median(IQR) in three age groups (PMA ≤ 31 weeks, PMA $\in (31-36]$ weeks, PMA > 36 weeks) as well as Pearson correlation coefficient with PMA.

Table 2. Overview of all computed features. Besides the first and the second order moments, the table reports all the relative and absolute power features in the frequency domain, namely the power in VLF, LF and HF bands, the ratio between the VLF and LF bands and between LF and HF bands and the normalized LF band power with respect to VLF band and HF band. The spectral features are reported for each the PSD estimation approaches that were used in this study. The last section reports the computed multifractal features, i.e. Hurst exponent (H_{exp}) and the (C_2) for the investigated scale ranges: $[j_1, j_2] = [3, 12]$ and $[j_1, j_2] = [5, 12]$.

Temporal features	
Statistical moments	μ_{RR}, σ_{RR}
Spectral features	
Welch	$P(VLF)$,$P(LF)$,$P(HF)$, $\frac{VLF}{LF}$,$\frac{LF}{HF}$,$\frac{LF}{LF+HF}$,$\frac{LF}{LF+VLF}$
SPWVD	$P(VLF)$,$P(LF)$,$P(HF)$, $\frac{VLF}{LF}$,$\frac{LF}{HF}$,$\frac{LF}{LF+HF}$,$\frac{LF}{LF+VLF}$
Wavelet	$P(VLF)$,$P(LF)$,$P(HF)$, $\frac{VLF}{LF}$,$\frac{LF}{HF}$,$\frac{LF}{LF+HF}$,$\frac{LF}{LF+VLF}$
Fractal features	
Multifractality	$H_{exp,[j_1,j_2=\mathbf{5},12]}$, $C_{2,[j_1,j_2=\mathbf{5},12]}$, $H_{exp,[j_1,j_2=3,12]}$,$C_{2,[j_1,j_2=3,12]}$

3 RESULTS

The overview of the dataset is reported in Table 1, which shows certain traits of the annotated bradycardias. The mean length is around 18 s. On average, there are 7 bradycardias per recording and the mean RR_i during bradycardias is approximately 631 ms. The overview shows that the infants have an average PMA of 34 weeks and 35 recordings are collected in the range (32-36] weeks. A total of 22 recordings is collected in the first days of life, while a set of 17 recording has been included from the weeks close to discharge. A detailed overview of each recording is reported in Table S1 and S2.

Figure 3 and Table 3 report the trends in the three different windowing schemes for the following features: the mean μ_{RR} and standard deviation of the *HRV* σ_{RR}, the absolute power in the LF band (and its logarithmic transform), the relative $\frac{LF}{LF+VLF}$ power, the Hurst Exponent in the range $[j_1, j_2] = [5, 12]$ $H_{exp_{[j_1,j_2=5,12]}}$ and the width of the singularity spectrum in the same range $C_{2_{[j_1,j_2=5,12]}}$. The overview of all features for all different windowing schemes (PB,BB and WB) are reported in the supplementary Tables S3, S4 and S5. Figure 3 reports the results for the windowing scheme for the within-bradycardia epochs on the left column, while the results for the between-bradycardia epochs are shown on the right column. The power in the LF band and the relative LF power ($\frac{LF}{LF+VLF}$) increase with increasing PMA in both scenarios: in particular, Pearson correlations ρ_{xy} are respectively 69% (72% with logarithm transform) and 64% for bradycardia epochs, while ρ_{xy} are respectively 71% (71% with logarithm transform) and 48% for between-bradycardia windows. Concerning the post=bradycardia period, the Table 3 shows a Pearson correlation of 69% for the power in LF band and 57% for $\frac{LF}{LF+VLF}$. Results are here reported for the wavelet approach, but the other spectral methodologies exhibit similar trends (see Tables S3, S4 and S5). In addition, the Hurst exponent (derived as the c_1 of the singularity spectrum) decreases with development (ρ_{xy} are -45% in the bradycardias scenario, -47% in post-bradycardia scenario and -50% in the between-bradycardia scenario), while the width of the singularity spectrum (c_2 parameter) increases with increasing PMA (ρ_{xy} are 54% in the bradycardia scenario, 45% in the post-bradycardia scenario and 43% in the between-bradycardia scenario). The greatest contrast was found with the variability of the heart-rate, σ_{RR}. While the standard deviation increases with infants' maturation in the between-bradycardia epochs, the σ_{RR} does not increase with age within the bradycardic event. Moreover, it is higher in the bradycardia epochs than in the between-bradycardia scenario ($\rho_{bradycardia} = -4\%$ vs $\rho_{between} = 64\%$ with $p_v = 0.77$ vs $p_v \leq 0.01$). The multifractal parameters are reported for $f_s = 8\ Hz$ in Table 3. A full overview of the effect of the sampling frequency on the fractal indices is reported in Table 4.

Table 5 shows the regression results for the linear mixed-effect models, while Table 6 reports the features selected by LASSO. Those two tables report the results for the three different windowing schemes (PB,BB,WB) in three different blocks, while the rows report the results for the different feature groups (temporal, spectral and fractal attributes) and sampling frequencies. The different columns respectively report the explained variance in the training set (R^2_{train}), the mean absolute error (MAE) and the explained variance in the test set (R^2_{test}). The best performance is reached for the combination of all features at $f_s = 12\ Hz$ in the PB scheme ($R^2_{train} = 0.75$, $MAE = 1.83\ weeks$, $R^2_{test} = 0.57$) as well as between bradycardias ($R^2_{train} = 0.68$, $MAE = 1.56\ weeks$, $R^2_{test} = 0.59$). During the bradycardia event (WB), the best performance is achieved with the

spectral features ($R^2_{train} = 0.73$, $MAE = 1.9\ weeks$, $R^2_{test} = 0.62$). Table 6 shows that the selected features are the absolute spectral power in LF and VLF together with C_2 parameter in the range $[j_1, j_2] = [5, 12]$ for the first two schemes. For the WB scheme, the selected feature is simply the power in LF band.

Figure 4 shows that the relationship of (10) between the H_{exp} and the ratios $\frac{VLF}{LF}$ and $\frac{LF}{HF}$. The first row shows the relationship between $\frac{VLF}{LF}$ and $H_{exp,[j_1,j_2=5,12]}$ in the three windowing schemes: WB in magenta circles, PB in light-blue squares and BB in indigo diamonds. The Pearson correlation coefficients are respectively 21%, 49% and 43%. The second row shows the relationship between $\frac{LF}{HF}$ and $H_{exp,[j_1,j_2=3,12]}$ in the same three schemes. The Pearson correlation coefficients are respectively 18%, 20% and 36%.

Table 3. The main temporal, spectral and fractal features are reported for the three windowing schemes (PB, BB and WB). The results are reported as median(IQR). IQR stands for *interquartile range*. The fractal indices are reported for $f_s = 8\ Hz$. The symbol ρ stands for the Pearson correlation coefficient. The symbol ** represents a significant correlation with $p \leq 0.01$ and $^{n.s.}$ is used to indicate a non-significant correlation.

Median(IQR) - PMA weeks	≤ 32	$(32-36]$	> 36	$\rho(\%)$
POST-bradycardia (PB) group				
μ_{RR}	374.65(366.38-391.36)	377.07(364.33-393.69)	387.2(374.98-416.44)	0.39**
σ_{RR}	16.71(12.02-22.05)	25.5(21.65-31.1)	28.47(24.03-32.08)	0.49**
$P(LF)_{Wavelet}$	2.14(0.96-3.68)	4.17(2.16-8.9)	17.74(4.94-25.51)	0.69**
$\frac{LF}{LF+VLF}_{Wavelet}$	5.38(3.45-8.7)	4.9(3.67-12.17)	14.06(11.77-18.09)	0.57**
$H_{exp,[j_1,j_2=5,12]}$	0.61(0.52-0.7)	0.55(0.45-0.59)	0.5(0.44-0.56)	-0.47**
$C_{2,[j_1,j_2=5,12]}$	-0.2(-0.26 - -0.17)	-0.19(-0.21 - -0.13)	-0.14(-0.15 - -0.11)	0.45**
BETWEEN-bradycardia (BB) group				
μ_{RR}	370.51(359.96-388.36)	377.42(363.11-389.25)	394.93(370.01-427.45)	0.47**
σ_{RR}	13.89(10.97-18.49)	19.81(15.72-23.82)	29.1(21.99-30.66)	0.64**
$P(LF)_{Wavelet}$	1.3(0.86-3.38)	4.23(1.93-6.28)	11.34(8.4-15)	0.71**
$\frac{LF}{LF+VLF}_{Wavelet}$	6.93(4.89-8.53)	7.9(4.63-11.05)	12.57(8.75-13.95)	0.48**
$H_{exp,[j_1,j_2=5,12]}$	0.6(0.52-0.68)	0.54(0.5-0.59)	0.48(0.45-0.52)	-0.5**
$C_{2,[j_1,j_2=5,12]}$	-0.19(-0.23 - -0.14)	-0.17(-0.2 - -0.14)	-0.09(-0.12 - -0.08)	0.43**
WITHIN-BRADYCARDIA (WB) group				
μ_{RR}	384.9(369.62-398.91)	384.16(369.2-397.51)	389.12(377.65-425.8)	0.37**
σ_{RR}	38.31(32.22-44.62)	40.61(32.5-49.81)	35.89(28.43-40.74)	$-0.04^{n.s.}$
$P(LF)_{Wavelet}$	2.3(1.12-4.03)	4.68(2.8-9.86)	18.66(5.35-26.46)	0.69**
$\frac{LF}{LF+VLF}_{Wavelet}$	2.57(1.13-3.97)	3.34(2.19-8.97)	10.96(6.69-16.78)	0.64**
$H_{exp,[j_1,j_2=5,12]}$	0.61(0.49-0.71)	0.55(0.43-0.62)	0.49(0.43-0.52)	-0.45**
$C_{2,[j_1,j_2=5,12]}$	-0.26(-0.3 - -0.21)	-0.21(-0.24 - -0.17)	-0.13(-0.18 - -0.11)	0.54**

4 DISCUSSION

This study provides an overview of autonomic nervous system maturation in preterm infants and aims to estimate the postmenstrual age of the infants based on the HRV. Since the neonatal tachogram is signal characterized by lack of stationarity and strong slow-wave baseline (Hoyer et al., 2013),(Abry et al., 2010),(Doret et al., 2015), the current study investigated the maturation of sympathetic and parasympathetic branches with the combination of temporal, spectral and fractal indices. Three main novel findings can be reported. First, Table 5 shows that the maturation of infants can be assessed with different spectral and fractal HRV indices with comparable performances to other

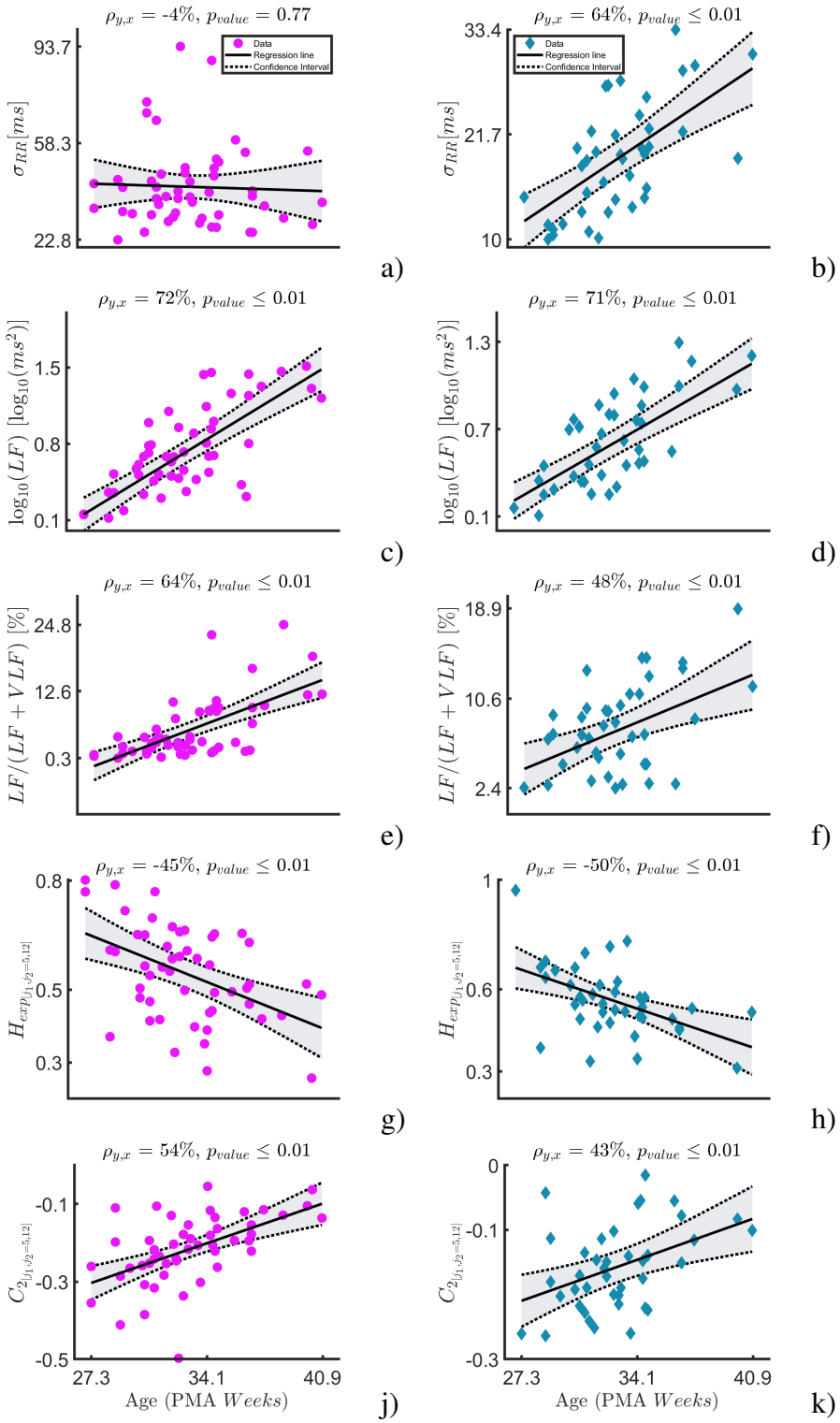


Figure 3. The figure shows the linear-mixed effect regressions between the post-menstrual age and the following HRV features: the standard deviation of the tachogram σ_{RR}, the absolute and the relative power in the LF band $\left(\log_{10}(LF), \frac{LF}{LF+VLF}\right)$, the Hurst exponent $H_{exp,[j_1,j_2=5,12]}$ and the parameter C_2. The sampling frequencies for the fractal indices is $f_s = 8\ Hz$. The left column - magenta circles report the results for the bradycardia epochs, while the right column - indigo diamonds the results for the between-bradycardia epochs. ρ is the correlation coefficient with the associated significance p_{value}.

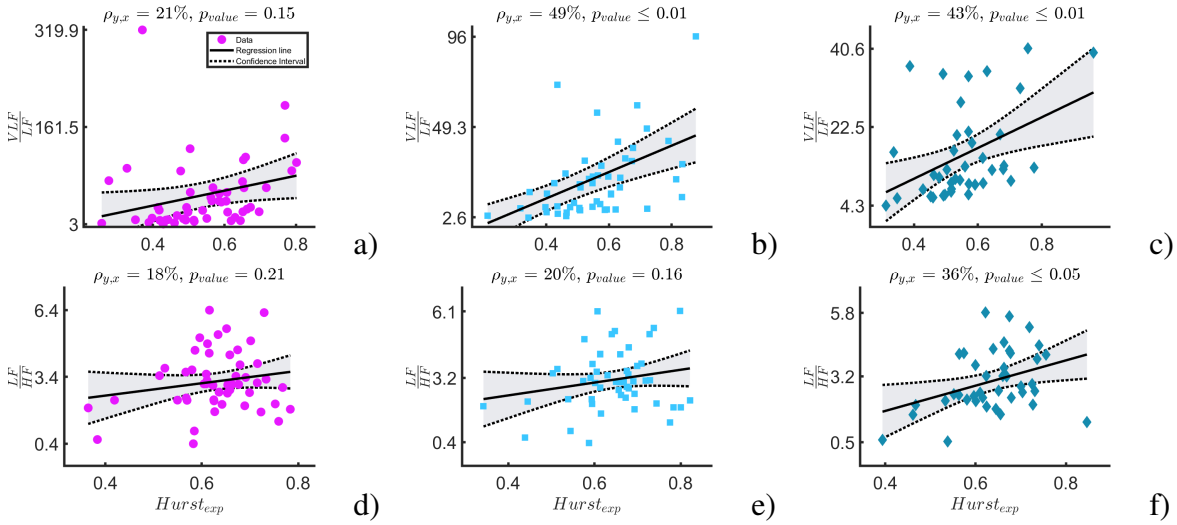


Figure 4. The figure shows results for the linear-mixed effect regression that models the relationship between $H_{exp,[j_1,j_2=5,12]}$ and $\frac{VLF}{LF}$ in the first row and between $H_{exp,[j_1,j_2=3,12]}$ and $\frac{LF}{HF}$ in the second row. The three columns respectively represents bradycardia epochs (magenta circle data points), post-bradycardia epochs (light-blue squares data points) and between-bradycardia epochs (indigo diamonds data points). ρ is the correlation coefficient of the regression and p_{value} represents the significance of the correlation.

maturation models for fetal and preterm development by (Hoyer et al., 2013) (De Wel et al., 2017), (Lavanga et al., 2017), (Lavanga et al., 2018). Second, Figure 4 reports that the spectral ratio $\frac{VLF}{LF}$ and the Hurst exponent in the range $[j_1, j_2] = [5, 12]$ are more correlated than the $\frac{LF}{HF}$ and the Hurst exponent $[j_1, j_2] = [3, 12]$. This might indicate that neonates do not have sympathovagal balance that rely on the typical interplay between LF and HF (Abry et al., 2010),(Doret et al., 2015). Third, the bradycardias can impact HRV maturational features, especially the most common temporal indices that are used in clinical practice, as highlighted in italic by the regression with only temporal features in the WB block of Table 5 and the correlation coefficients in Table 3. Additionally, the relationship between spectral ratios and H_{exp} is strongly diminished in the WB scheme, as stressed by Figure 4.

The different age models that were derived in this study can outperform or can be compared to the other developmental models reported in the literature (Hoyer et al., 2013), (Lavanga et al., 2018). Specifically, Table 5 highlights the capacity of spectral features to outperform all other features in the PMA estimation in all three windowing schemes ($R^2_{train} = [0.74, 0.59, 0.72]$, $R^2_{test} = [0.57, 0.69, 0.62]$, $MAE = [1.83, 1.56, 1.9]$ $Weeks$). Furthermore, the LF power is consistently selected by LASSO for all the different f_s and with any type of windowing scheme. These results are not simply in line with decrease of $\frac{VLF}{LF}$ by (Hoyer et al., 2013), but they are also supported by other clinical findings. Namely, an increase of the short-term variability of the tachogram was found during first days of life (De Souza Filho et al., 2019) and the absolute LF power can discriminate preterm and full term infants with 84% accuracy (Mulkey et al., 2018). However, the highest performances in the PB and BB schemes are achieved when the fractal and spectral features are combined, as highlighted in bold in Table 5 and suggested by the concomitant increase of entropy and short-term variability of HRV found by (De Souza Filho et al., 2019). Interestingly,

Table 4. The fractal features are reported in three different age categories and for the investigated sampling frequencies $f_s = [6, 8, 12]\ Hz$. The results are reported as median(IQR) for the between-bradycardia and bradycardia periods. IQR stands for *interquartile range*. The symbol ρ stands for the Pearson correlation coefficient. The symbol ** represents a significant correlation with $p \leq 0.01$, and * is used for a significant correlation with $p \leq 0.05$. $^{n.s.}$ is used to indicate a non-significant correlation.

Median(IQR) - PMA weeks	≤ 32	$(32-36]$	> 36	$\rho(\%)$
Fractal features in the PB group, $f_s = 6\ Hz$				
$H_{exp,[j_1,j_2=5,12]}$	0.53(0.46-0.67)	0.49(0.41-0.58)	0.45(0.36-0.5)	-0.45**
$C_{2,[j_1,j_2=5,12]}$	-0.2(-0.25 - -0.18)	-0.19(-0.22 - -0.15)	-0.13(-0.17 - -0.1)	0.57**
$H_{exp,[j_1,j_2=3,12]}$	0.65(0.56-0.71)	0.6(0.55-0.68)	0.56(0.53-0.6)	-0.4**
$C_{2,[j_1,j_2=3,12]}$	-0.17(-0.18 - -0.13)	-0.13(-0.16 - -0.11)	-0.09(-0.12 - -0.08)	0.41**
Fractal features in the PB group, $f_s = 8\ Hz$				
$H_{exp,[j_1,j_2=5,12]}$	0.61(0.52-0.7)	0.55(0.45-0.59)	0.5(0.44-0.56)	-0.47**
$C_{2,[j_1,j_2=5,12]}$	-0.2(-0.26 - -0.17)	-0.19(-0.21 - -0.13)	-0.14(-0.15 - -0.11)	0.45**
$H_{exp,[j_1,j_2=3,12]}$	0.67(0.6-0.71)	0.66(0.59-0.69)	0.62(0.58-0.65)	-0.33*
$C_{2,[j_1,j_2=3,12]}$	-0.14(-0.16 - -0.1)	-0.11(-0.14 - -0.08)	-0.09(-0.11 - -0.09)	0.2$^{n.s.}$
Fractal features in the PB group, $f_s = 12\ Hz$				
$H_{exp,[j_1,j_2=5,12]}$	0.62(0.52-0.7)	0.56(0.49-0.64)	0.53(0.44-0.54)	-0.45**
$C_{2,[j_1,j_2=5,12]}$	-0.2(-0.23 - -0.16)	-0.17(-0.19 - -0.15)	-0.11(-0.13 - -0.1)	0.57**
$H_{exp,[j_1,j_2=3,12]}$	0.67(0.61-0.73)	0.64(0.61-0.71)	0.62(0.6-0.63)	-0.33*
$C_{2,[j_1,j_2=3,12]}$	-0.13(-0.15 - -0.11)	-0.11(-0.13 - -0.09)	-0.09(-0.11 - -0.08)	0.22$^{n.s.}$

Median(IQR) - PMA weeks	≤ 32	$(32-36]$	> 36	$\rho(\%)$
Fractal features in the BB group, $f_s = 6\ Hz$				
$H_{exp,[j_1,j_2=5,12]}$	0.55(0.45-0.65)	0.52(0.43-0.55)	0.45(0.4-0.48)	-0.43**
$C_{2,[j_1,j_2=5,12]}$	-0.19(-0.24 - -0.16)	-0.17(-0.2 - -0.13)	-0.11(-0.12 - -0.09)	0.52**
$H_{exp,[j_1,j_2=3,12]}$	0.65(0.56-0.69)	0.61(0.57-0.67)	0.55(0.52-0.59)	-0.39*
$C_{2,[j_1,j_2=3,12]}$	-0.15(-0.17 - -0.12)	-0.13(-0.15 - -0.1)	-0.08(-0.1 - -0.06)	0.39*
Fractal features in the BB group, $f_s = 8\ Hz$				
$H_{exp,[j_1,j_2=5,12]}$	0.6(0.52-0.68)	0.54(0.5-0.59)	0.48(0.45-0.52)	-0.5**
$C_{2,[j_1,j_2=5,12]}$	-0.19(-0.23 - -0.14)	-0.17(-0.2 - -0.14)	-0.09(-0.12 - -0.08)	0.43**
$H_{exp,[j_1,j_2=3,12]}$	0.68(0.61-0.73)	0.65(0.6-0.67)	0.6(0.55-0.62)	-0.36*
$C_{2,[j_1,j_2=3,12]}$	-0.12(-0.15 - -0.1)	-0.12(-0.14 - -0.1)	-0.08(-0.09 - -0.05)	0.23$^{n.s.}$
Fractal features in the BB group, $f_s = 12\ Hz$				
$H_{exp,[j_1,j_2=5,12]}$	0.62(0.52-0.68)	0.57(0.52-0.63)	0.52(0.48-0.53)	-0.43**
$C_{2,[j_1,j_2=5,12]}$	-0.18(-0.23 - -0.16)	-0.15(-0.19 - -0.12)	-0.09(-0.11 - -0.08)	0.53**
$H_{exp,[j_1,j_2=3,12]}$	0.68(0.6-0.71)	0.64(0.6-0.69)	0.59(0.54-0.64)	-0.31$^{n.s.}$
$C_{2,[j_1,j_2=3,12]}$	-0.12(-0.14 - -0.11)	-0.11(-0.12 - -0.1)	-0.08(-0.1 - -0.06)	0.26$^{n.s.}$

Median(IQR) - PMA weeks	≤ 32	$(32-36]$	> 36	$\rho(\%)$
Fractal features in the WB period, $f_s = 6\ Hz$				
$H_{exp,[j_1,j_2=5,12]}$	0.52(0.42-0.7)	0.48(0.39-0.52)	0.43(0.4-0.46)	-0.36**
$C_{2,[j_1,j_2=5,12]}$	-0.23(-0.29 - -0.2)	-0.21(-0.24 - -0.17)	-0.14(-0.18 - -0.12)	0.55**
$H_{exp,[j_1,j_2=3,12]}$	0.62(0.58-0.67)	0.6(0.53-0.63)	0.57(0.5-0.6)	-0.31*
$C_{2,[j_1,j_2=3,12]}$	-0.19(-0.23 - -0.15)	-0.16(-0.19 - -0.14)	-0.1(-0.12 - -0.09)	0.48**
Fractal features in the WB period, $f_s = 8\ Hz$				
$H_{exp,[j_1,j_2=5,12]}$	0.61(0.49-0.71)	0.55(0.43-0.62)	0.49(0.43-0.52)	-0.45**
$C_{2,[j_1,j_2=5,12]}$	-0.26(-0.3 - -0.21)	-0.21(-0.24 - -0.17)	-0.13(-0.18 - -0.11)	0.54**
$H_{exp,[j_1,j_2=3,12]}$	0.66(0.62-0.71)	0.64(0.58-0.68)	0.61(0.58-0.62)	-0.36**
$C_{2,[j_1,j_2=3,12]}$	-0.15(-0.2 - -0.12)	-0.14(-0.17 - -0.11)	-0.11(-0.12 - -0.09)	0.31*
Fractal features in the WB period, $f_s = 12\ Hz$				
$H_{exp,[j_1,j_2=5,12]}$	0.58(0.5-0.68)	0.56(0.5-0.6)	0.5(0.49-0.53)	-0.36**
$C_{2,[j_1,j_2=5,12]}$	-0.22(-0.28 - -0.19)	-0.19(-0.22 - -0.17)	-0.12(-0.14 - -0.1)	0.58**
$H_{exp,[j_1,j_2=3,12]}$	0.64(0.61-0.68)	0.65(0.61-0.68)	0.63(0.6-0.65)	-0.18$^{n.s.}$
$C_{2,[j_1,j_2=3,12]}$	-0.16(-0.18 - -0.11)	-0.13(-0.16 - -0.11)	-0.11(-0.11 - -0.09)	0.32*

the highest performances are also achieved when the between bradycardias epochs are considered ($MAE = 1.56\ Weeks$), which further reveals a bias effect of bradycardias in the description of

Table 5. Linear mixed-effect model performances. For each feature set and sampling frequency f_s, the table shows the median(IQR) over the 20 iterations for R^2_{train} on the train set as well as R^2_{test} and the MAE in weeks on test set. IQR here stands for the difference between 25% and 75% quantiles.

Post-bradycardia (PB) epochs			
Feature type $\|_{fs}$	R^2_{train}	$MAE(weeks)$	R^2_{test}
All features $\|_{6Hz}$	0.73(0.11)	1.88(0.39)	0.57(0.29)
All features $\|_{8Hz}$	0.75(0.1)	1.85(0.3)	0.56(0.23)
All features $\|_{12Hz}$	0.75(0.09)	**1.83(0.41)**	0.57(0.22)
Temporal features	0.44(0.28)	2(0.56)	0.35(0.19)
Spectral features	0.74(0.12)	2.01(0.42)	0.5(0.11)
Fractal features $\|_{6Hz}$	0.33(0.17)	2.21(0.42)	0.33(0.34)
Fractal features $\|_{8Hz}$	0.35(0.13)	2.31(0.54)	0.21(0.22)
Fractal features $\|_{12Hz}$	0.26(0.1)	2.18(0.46)	0.43(0.28)
Between-bradycardia (BB) epochs			
Feature type $\|_{fs}$	R^2_{train}	$MAE(weeks)$	R^2_{test}
All features $\|_{6Hz}$	0.55(0.12)	1.82(0.28)	0.57(0.24)
All features $\|_{8Hz}$	0.6(0.11)	1.81(0.38)	0.55(0.19)
All features $\|_{12Hz}$	0.68(0.11)	**1.56(0.39)**	0.59(0.16)
Temporal features	0.6(0.33)	2.06(0.38)	0.44(0.24)
Spectral features	0.59(0.19)	1.93(0.54)	0.59(0.15)
Fractal features $\|_{6Hz}$	0.3(0.22)	2.57(0.43)	0.15(0.19)
Fractal features $\|_{8Hz}$	0.22(0.26)	2(0.25)	0.24(0.36)
Fractal features $\|_{12Hz}$	0.34(0.28)	2.16(0.53)	0.18(0.31)
Within-Bradycardia (WB) epochs			
Feature type $\|_{fs}$	R^2_{train}	$MAE(weeks)$	R^2_{test}
All features $\|_{6Hz}$	0.73(0.1)	1.97(0.42)	0.58(0.25)
All features $\|_{8Hz}$	0.7(0.15)	1.91(0.21)	0.5(0.25)
All features $\|_{12Hz}$	0.72(0.15)	1.95(0.33)	0.57(0.24)
Temporal features	*0.14(0.1)*	*2.79(0.35)*	*0.13(0.13)*
Spectral features	0.73(0.17)	**1.9(0.21)**	0.62(0.21)
Fractal features $\|_{6Hz}$	0.33(0.07)	2.16(0.4)	0.23(0.18)
Fractal features $\|_{8Hz}$	0.36(0.13)	2.03(0.56)	0.43(0.22)
Fractal features $\|_{12Hz}$	0.4(0.16)	2.13(0.56)	0.29(0.28)

autonomic maturation. In line with (Hoyer et al., 2013),(Longin et al., 2006),(Clairambault et al., 1992),(Curzi-Dascalova, 1994), we found that the tachogram mean μ_{RR} and its standard deviation σ_{RR} increase with maturation together with the absolute power in all investigated frequency bands. If the relative power is considered, both $\frac{LF}{VLF+LF}$ and $\frac{LF}{HF+LF}$ increase with age (Table 3 and supplementary Tables S3, S4 and S5), which means the spectral ratios $\frac{VLF}{LF}$ and $\frac{LF}{HF}$ had opposite directions. While the latter increases with age, we also found that $\frac{VLF}{LF}$ decreases as shown by (Hoyer et al., 2013). It should be stressed that the relative power features are less correlated with age (see suppplementary Tables S3, S4 and S5) and they are never selected in the LASSO procedure (Table 6). These results confirm the findings by (Longin et al., 2006) and (Curzi-Dascalova, 1994),

Table 6. LASSO selected features for the linear mixed-effect model. For each feature set, the features that have been selected more than 40% of times have been reported. σ_{RR} and μ_{RR} stand for the standard deviation and the mean of HRV. $log_{10}(LF)$, $log_{10}(VLF)$,$\frac{VLF}{LF}$ stand for the absolute power in the LF and VLF bands and the ratio between the two. Results are reported for the Wigner-Ville distribution (SPWD) or the wavelet transform. $H_{exp,[j_2,j_2]}$ and $c_{2,[j_2,j_2]}$ stand for the Hurst exponent and the parameter c_2 in the range $[j_1, j_2]$.

Post-bradycardia (PB) epochs				
Feature type	$\vert_{fs}$			
All	$\vert_{6Hz}$	$\log_{10}(LF)_{SPWVD}$	$\log_{10}(LF)_{Wavelet}$	$C_{2,[j_1,j_2=5,12]}$
All	$\vert_{8Hz}$	$\log_{10}(LF)_{Wavelet}$		
All	$\vert_{12Hz}$	$\log_{10}(LF)_{SPWVD}$	$C_{2,[j_1,j_2=\mathbf{5},12]}$	
Spectral		$\log_{10}(LF)_{SPWVD}$	$\log_{10}(LF)_{Wavelet}$	
Fractal	$\vert_{6Hz}$	$C_{2,[j_1,j_2=\mathbf{5},12]}$		
Fractal	$\vert_{8Hz}$	$H_{exp,[j_1,j_2=\mathbf{5},12]}$	$C_{2,[j_1,j_2=\mathbf{5},12]}$	
Fractal	$\vert_{12Hz}$	$C_{2,[j_1,j_2=\mathbf{5},12]}$		
Between-bradycardia (BB) epochs				
Feature type	$\vert_{fs}$			
All	$\vert_{6Hz}$	μ_{RR}	$\log_{10}(LF)_{SPWVD}$	
All	$\vert_{8Hz}$	$\log_{10}(LF)_{SPWVD}$		
All	$\vert_{12Hz}$	$\log_{10}(VLF)_{Wavelet}$	$\log_{10}(LF)_{SPWVD}$	$C_{2,[j_1,j_2=\mathbf{5},12]}$
Spectral		$\log_{10}(LF)_{SPWVD}$		
Fractal	$\vert_{6Hz}$	$H_{exp,[j_1,j_2=\mathbf{5},12]}$	$C_{2,[j_1,j_2=\mathbf{5},12]}$	$H_{exp,[j_1,j_2=3,12]}$
		$C_{2,[j_1,j_2=3,12]}$		
Fractal	$\vert_{8Hz}$	$H_{exp,[j_1,j_2=\mathbf{5},12]}$		
Fractal	$\vert_{12Hz}$	$C_{2,[j_1,j_2=\mathbf{5},12]}$		
Within-Bradycardia (WB) epochs				
Feature type	$\vert_{fs}$			
All	$\vert_{6Hz}$	$\log_{10}(LF)_{Wavelet}$	$C_{2,[j_1,j_2=\mathbf{5},12]}$	$C_{2,[j_1,j_2=3,12]}$
All	$\vert_{8Hz}$	$\log_{10}(LF)_{Wavelet}$	$C_{2,[j_1,j_2=\mathbf{5},12]}$	
All	$\vert_{12Hz}$	$\log_{10}(LF)_{Wavelet}$	$C_{2,[j_1,j_2=\mathbf{5},12]}$	
Spectral		$\log_{10}(LF)_{Wavelet}$		
Fractal	$\vert_{6Hz}$	$C_{2,[j_1,j_2=\mathbf{5},12]}$	$C_{2,[j_1,j_2=3,12]}$	
Fractal	$\vert_{8Hz}$	$H_{exp,[j_1,j_2=\mathbf{5},12]}$	$C_{2,[j_1,j_2=\mathbf{5},12]}$	
Fractal	$\vert_{12Hz}$	$H_{exp,[j_1,j_2=\mathbf{5},12]}$	$C_{2,[j_1,j_2=\mathbf{5},12]}$	

who found also greater increase in the absolute power during maturation, and the findings by (Mulkey et al., 2018), which also displays the superiority of the absolute power in the classification between preterm and full-term neonates compared to the relative indices. The lack of stationarity and the $1/f$ spectrum behavior makes difficult to describe the autonomic maturation without all the frequency bands in place. Furthermore, the regularity measure by the fractal indices with the H_{exp} and c_2 decreases with development and they play a role in the age estimation models (Table 6).

These findings seem to suggest that the ratio $\frac{LF}{HF}$ might not be the best suitable index for the sympathovagal balance and the common HRV frequency bands are suitable for infants. As anticipated, David et al. noticed that the fetal heart-rate has such enhanced slow-wave baseline, which increases the power in the VLF band, such that both Hoyer et al. and David et al. used the ratio $\frac{VLF}{LF}$ as a possible index to describe the sympatho-vagal interplay (David et al., 2007), (Hoyer et al., 2013). This approach seems confirmed by the results in Figure 4. As discussed by Abry (Abry et al., 2010)

and Doret (Doret et al., 2015), the spectral ratio is linked to H_{exp} via (10). The panels suggest that the ANS modulation and its fractal regularity lie in the lower-frequency bands, since the H_{exp} is more correlated with $\frac{VLF}{LF}$. The Pearson correlation coefficients ρ_{xy} between $\frac{VLF}{LF}$ and H are respectively 21%,49%,43% according to different windowing schemes compared to ρ_{xy} between $\frac{LF}{HF}$ and H_{exp} (18%, 20% and 36%). It is important to notice that the H_{exp} matches the spectral ratio if its estimation range $[j_1, j_2]$ matches the frequency bands with most of the exponential decay in the PSD. In this study, $[j_1, j_2 = 5, 12]$ covers specifically the lower frequency bands and its importance is confirmed by the features selected by LASSO (Table 6). In line with Doret (Doret et al., 2015), the current findings clearly suggest a redefinition of $\frac{LF}{HF}$ with an extension of frequency bands from the most common adults' range, e.g. $LF = [0.02 - 0.15]\ Hz$ and $HF = [0.15 - 1.3]\ Hz$. They also highlights the greater prominence of the slower oscillations in the description of premature ANS.

However, the results also highlight the disruptive role of bradycardias in maturation analysis. As anticipated, the best regression results are achieved in the between bradycardia epochs (Table 5) and the relationship between the spectral ratios and the H_{exp} is disrupted with WB windowing (panels with magenta circle 4). Most importantly, the relationship between the temporal features and maturation is lost, as highlighted by the poor R^2 (Table 5 and panels with magenta circles in Figure 3). In addition, Gee et al. (Gee et al., 2017) observed that the LF power, the variance and the regularity of the heart-rate increase before bradycardias. The results in Figure 3 and Tables S4, S5 support this increase in variance and regularity (as can be easily noticed by the y-axis of σ_{RR} or any other features of the left column in Figure 3). This finding clearly implies that exclusion of bradycardias is fundamental whenever using the standard deviation and the mean of the tachogram to assess the maturation of ANS. Figure 4 also shows that bradycardias annihilate the expected relationship between the spectral ratios and the Hurst exponent. This is a further proof that bradycardias disrupt the vagal tone (Porges, 1995), which can distort the PSD power-law in Equation 8. However, table 5 shows that the autonomic age models within bradycardia can maintain comparable performance to the other two windowing schemes thanks to the spectral features. In particular, Table 6 confirms that the most selected power attribute is the power in $LF = [0.08 - 0.2]$ Hz, as further proof of the central role of this range in the bradycardic event and ANS maturation (Gee et al., 2017), (David et al., 2007), (Hoyer et al., 2013).

It is also important to highlight some limitations of the current study. Bolea have shown a dependency for nonlinear metrics (such as Sample Entropy) with the resampling frequency of the tachogram (Bolea et al., 2016). Based on their results, Bolea et al. concluded that a resampling frequency correction of nonlinear parameters is needed in cardiovascular applications in order to detect meaningful results (such as experiments with body position changes) (Bolea et al., 2016). The employed fractal indices clearly show a increasing trend with an increasing sampling frequency (Section 2.3.3 and Table 4). However, a correction for the sampling frequency was not implemented. The multifractal properties were investigated with different sampling frequencies and our study seems to show mild differences in term of regression results and correlation with age (Table 4). One may also object the exclusion of proper sleep-staging in the current analysis, as normally done by (Curzi-Dascalova, 1994). However, the specific focus on the bradycardia effect strongly limit the number of the windows available. On top of that, bradycardias are events normally associated

to active sleep (Porges, 1995) and most of the annotated bradycardias in this study were found during states that were not associated to quiet sleep. Similarly, one may also find the number of patients limited, but it was caused by the difficulties in the follow-up. All the included patients had normal developmental outcome at 2 years and the development assessment process is normally characterized by large drop-outs. Concerning the methodology, the different spectral methods (Welch, Wavelet and Wigner-Ville) show very similar spectral trends, but LASSO more frequently tends to select time-frequency distribution features (Wavelet and Wigner-Ville, Table S4, S5). Although there are studies that claim the superiority of the quadratic time-frequency methods (Widjaja et al., 2013),(Orini et al., 2012), the current findings show the wavelet approach would suffice for the spectral analysis.

In a nutshell, the HRV analysis might a useful tool for development monitoring, but two important factors have to be taken into account. First, the neonatal HRV is characterized by a very-low frequency tone which requires a redefinition of the different frequency bands to the autonomic stimulation. Second, bradycardia have a disruptive role in the assessment of maturation.

5 CONCLUSION

The present study investigated the maturation of the preterm autonomic nervous system by means of temporal, spectral and fractal features of HRV. Three main findings can be reported. First, infants' maturation can be described by means of multifractal and spectral analysis, which show an increasing trend of LF power as well as decreasing trend of fractal regularity with increasing post-menstrual age. The best obtained regression performances ($R^2 = 0.68$ and $MAE = 1.56$ $weeks$) are obtained as combination of fractal and spectral features and are comparable to other developmental models reported by different authors (Hoyer et al., 2013), (Lavanga et al., 2017), (Lavanga et al., 2018), (De Wel et al., 2017). Second, this predominance of LF and VLF bands as well as the lower scales for the multifractal indices suggest that the sympathovagal balance of neonates might not simply be related to the ratio $\frac{LF}{HF}$, but the entire HRV band and the regularity of the tachogram should be included to have better understanding of the ANS maturation. Third, bradycardias might forcefully increase the variance of the heart-rate and disrupt the relationship between autonomic indices and age. The PMA estimation models based on novel HRV indices provides a more comprehensive understanding of postnatal autonomic maturation. They can be also considered an alternative automated maturity index to other electrophysiological data analysis for the NICU. This research might be a first step to design personalized therapies or preventive care to preserve infants' development.

CONFLICT OF INTEREST STATEMENT

The authors declare that the research was conducted in the absence of any commercial or financial relationships that could be construed as a potential conflict of interest.

AUTHOR CONTRIBUTIONS

ML wrote the article and conducted the data analysis. EM and JM supported the data analysis. AC and SVH supervised the data analysis. KJ and GN conducted the data collection. EM, JM, BB, KJ, EO, GN, SVH and AC reviewed and corrected the manuscript. All authors contributed to the article and approved the submitted version.

FUNDING

Research supported by Bijzonder Onderzoeksfonds KU Leuven (BOF) : C24/15/036 "The effect of perinatal stress on the later outcome in preterm babies", EU: H2020 MSCA-ITN-2018: 'INtegrating Functional Assessment measures for Neonatal Safeguard (INFANS)', funded by the European Commission under Grant Agreement #813483. This research received funding from the Flemish Government (AI Research Program). SVH and ML are affiliated to Leuven.AI - KU Leuven institute for AI, B-3000, Leuven, Belgium. Funders were not involved in the study design, collection, analysis, interpretation of data, the writing of this article or the decision to submit it for publication

ACKNOWLEDGMENTS

Mario Lavanga is a SB Ph.D. fellow at Fonds voor Wetenschappelijk Onderzoek (FWO), Vlaanderen, supported by the Flemish government. SVH and ML are affiliated to Leuven.AI - KU Leuven institute for AI, B-3000, Leuven, Belgium.

DATA AVAILABILITY STATEMENT

The datasets presented in this article are not readily available because the clinical metadata of patients (such as hospital ID, age, recording time-stamps, pain scales) are subject to the European data-privacy policy. Requests to access the datasets should be directed to mlavanga@esat.kuleuven.be. The authors will try to provide an anonimized version of dataset in compliance with the privacy policy of the University Hospitals of Leuven, which is the owner of the data.

REFERENCES

Abry, P., Wendt, H., Jaffard, S., Helgason, H., Goncalves, P., Pereira, E., et al. (2010). Methodology for multifractal analysis of heart rate variability: From LF/HF ratio to wavelet leaders. In *2010 Annual International Conference of the IEEE Engineering in Medicine and Biology* (IEEE), 106–109. doi:10.1109/IEMBS.2010.5626124

Atkinson, E. and Fenton, A. C. (2009). Management of apnoea and bradycardia in neonates. *Paediatrics and Child Health* 19, 550–554. doi:10.1016/J.PAED.2009.06.008

Aylward, G. P. (2014). Neurodevelopmental outcomes of infants born prematurely. *Journal of Developmental and Behavioral Pediatrics* 35, 394–407. doi:10.1097/01.DBP.0000452240.39511.d4

Bolea, J., Pueyo, E., Orini, M., and Bailón, R. (2016). Influence of Heart Rate in Non-linear HRV Indices as a Sampling Rate Effect Evaluated on Supine and Standing. *Frontiers in Physiology* 7, 501. doi:10.3389/fphys.2016.00501

Camm, A., Malik, M., Bigger, J., and Günter, B. (1996). Task force of the European Society of Cardiology and the North American Society of Pacing and Electrophysiology. Heart rate variability: standards of measurement, physiological interpretation and clinical use. *Circulation* 93, 1043–1065

Clairambault, J., Curzi-dascalovab, L., Kauffmann, F., and Mkdiguea, C. (1992). Heart Rate Variability in Normal Sleeping and Preterm Neonates Full-Term. *Early Human Development* 28, 169–183

Curzi-Dascalova, L. (1994). Development of sleep and autonomic nervous system contorl in premature and full-term newborns. *Archives de pediatrie* 2, 255–262. doi:10.1016/0929-693X(96)81138-9

David, M., Hirsch, M., Karin, J., Toledo, E., and Akselrod, S. (2007). An estimate of fetal autonomic state by time-frequency analysis of fetal heart rate variability. *Journal of Applied Physiology* 102

De Souza Filho, L. F. M., De Oliveira, J. C. M., Ribeiro, M. K. A., Moura, M. C., Fernandes, N. D., De Sousa, R. D., et al. (2019). Evaluation of the autonomic nervous system by analysis of heart rate variability in the preterm infants. *BMC Cardiovascular Disorders* 19, 198. doi:10.1186/s12872-019-1166-4

De Wel, O., Lavanga, M., Dorado, A., Jansen, K., Dereymaeker, A., Naulaers, G., et al. (2017). Complexity Analysis of Neonatal EEG Using Multiscale Entropy: Applications in Brain Maturation and Sleep Stage Classification. *Entropy* 19, 516. doi:10.3390/e19100516

Dereymaeker, A., Pillay, K., Vervisch, J., Van Huffel, S., Naulaers, G., Jansen, K., et al. (2017). An Automated Quiet Sleep Detection Approach in Preterm Infants as a Gateway to Assess Brain Maturation. *International Journal of Neural Systems* 27, 1750023. doi:10.1142/S012906571750023X

Doret, M., Spilka, J., Chudáček, V., Gonçalves, P., Abry, P., and Stanley, H. (2015). Fractal Analysis and Hurst Parameter for Intrapartum Fetal Heart Rate Variability Analysis: A Versatile Alternative to Frequency Bands and LF/HF Ratio. *PLOS ONE* 10, e0136661. doi:10.1371/journal.pone.0136661

Franke, K., Luders, E., May, A., Wilke, M., and Gaser, C. (2012). Brain maturation: predicting individual BrainAGE in children and adolescents using structural MRI. *Neuroimage* 63, 1305–1312. doi:10.1016/j.neuroimage.2012.08.001

Gee, A. H., Barbieri, R., Paydarfar, D., and Indic, P. (2017). Predicting Bradycardia in Preterm Infants Using Point Process Analysis of Heart Rate. *IEEE Transactions on Biomedical Engineering* 64, 2300–2308. doi:10.1109/TBME.2016.2632746

Hoyer, D., Tetschke, F., Jaekel, S., Nowack, S., Witte, O. W., Schleußner, E., et al. (2013). Fetal Functional Brain Age Assessed from Universal Developmental Indices Obtained from Neuro-Vegetative Activity Patterns. *PLoS ONE* 8, 1–8. doi:10.1371/journal.pone.0074431

Ivanov, P. C., Amaral, L. a., Goldberger, a. L., Havlin, S., Rosenblum, M. G., Struzik, Z. R., et al. (1999). Multifractality in human heartbeat dynamics. *Nature* 399, 461–465. doi:10.1038/20924

Javorka, K., Lehotska, Z., Kozar, M., Uhrikova, Z., Kolarovszki, B., Javorka, M., et al. (2017). Heart Rate Variability in Newborns. *Physiol. Res* 66, 203–214. doi:10.33549/physiolres.933676

Karin, J., Hirsch, M., and Akselrod, S. (1993). An estimate of fetal autonomic state by spectral analysis of fetal heart rate fluctuations. *Pediatric Research* 34, 134–138. doi:10.1203/00006450-199308000-00005

Koolen, N., Dereymaeker, A., Räsänen, O., Jansen, K., Vervisch, J., Matic, V., et al. (2016). Early development of synchrony in cortical activations in the human. *Neuroscience* 322, 298–307. doi:10.1016/j.neuroscience.2016.02.017

Krueger, C., van Oostrom, J. H., and Shuster, J. (2010). A Longitudinal Description of Heart Rate Variability in 28–34-Week-Old Preterm Infants. *Biological Research For Nursing* 11, 261–268. doi:10.1177/1099800409341175

Lavanga, M., De Wel, O., Caicedo, A., Jansen, K., Dereymaeker, A., Naulaers, G., et al. (2017). Monitoring Effective Connectivity in the Preterm Brain: A Graph Approach to Study Maturation. *Complexity* 2017. doi:10.1155/2017/9078541

Lavanga, M., Wel, O. D., Caicedo, A., Jansen, K., Dereymaeker, A., Naulaers, G., et al. (2018). A brain-age model for preterm infants based on functional connectivity. *Physiological Measurement* 39, 044006. doi:10.1088/1361-6579/AABAC4

Leonarduzzi, R. F., Schlotthauer, G., and Torres, M. E. (2010). Wavelet leader based multifractal analysis of heart rate variability during myocardial ischaemia. *2010 Annual International Conference of the IEEE Engineering in Medicine and Biology* , 110–113doi:10.1109/IEMBS.2010.5626091

Longin, E., Gerstner, T., Schaible, T., Lenz, T., and König, S. (2006). Maturation of the autonomic nervous system: Differences in heart rate variability in premature vs. term infants. *Journal of Perinatal Medicine* 34, 303–308. doi:10.1515/JPM.2006.058

Mazursky, J. E., Birkett, C. L., Bedell, K. A., Ben-Haim, S. A., and Segar, J. L. (1998). Development of baroreflex influences on heart rate variability in preterm infants. *Early Human Development* 53, 37–52. doi:10.1016/S0378-3782(98)00038-3

Moeyersons, J., Amoni, M., Huffel, S. V., Willems, R., and Varon, C. (2019). R-DECO: An open-source Matlab based graphical user interface for the detection and correction of R-peaks. *bioRxiv* , 560706doi:10.1101/560706

Mulkey, S. B., Kota, S., Swisher, C. B., Hitchings, L., Metzler, M., Wang, Y., et al. (2018). Autonomic nervous system depression at term in neurologically normal premature infants. *Early Human Development* 123, 11–16. doi:10.1016/j.earlhumdev.2018.07.003

Orini, M., Bailon, R., Mainardi, L. T., Laguna, P., and Flandrin, P. (2012). Characterization of dynamic interactions between cardiovascular signals by time-frequency coherence. *IEEE Transactions on Biomedical Engineering* 59, 663–673. doi:10.1109/TBME.2011.2171959

Paolillo, P. and Picone, S. (2013). Apnea of prematurity. *Journal of Pediatric and Neonatal Individualized Medicine* 2. doi:10.7363/020213

Popivanov, D., Stomonyakov, V., Minchev, Z., Jivkova, S., Dojnov, P., Jivkov, S., et al. (2006). Multifractality of decomposed EEG during imaginary and real visual-motor tracking. *Biological Cybernetics* 94, 149–156. doi:10.1007/s00422-005-0037-5

Porges, S. W. (1995). Orienting in a defensive world: Mammalian modifications of our evolutionary heritage. A Polyvagal Theory. *Psychophysiology* 32, 301–318. doi:10.1111/j.1469-8986.1995.tb01213.x

Smith, S. L., Haley, S., Slater, H., and Moyer-Mileur, L. J. (2013). Heart rate variability during caregiving and sleep after massage therapy in preterm infants. *Early Human Development* 89, 525–529. doi:10.1016/j.earlhumdev.2013.01.004

Wendt, H., Abry, P., and Jaffard, S. (2007). Bootstrap for Multifractal Analysis. *IEEE Signal Processing Magazine* 24, 38–48. doi:10.1109/MSP.2007.4286563

Widjaja, D., Orini, M., Vlemincx, E., and Huffel, S. V. (2013). Cardiorespiratory Dynamic Response to Mental Stress: A Multivariate Time-Frequency Analysis. *Computational and Mathematical Methods in Medicine* doi:10.1155/2013/451857

SUPPLEMENTARY MATERIAL

Table S1. A detail overview of the recordings of the included patients: the study of each patient ID (PAT_{ID}), the serial number that indicates the recording for each patient (REC_{ID}), the duration of the recording in minutes ($Duration_{Rec}$), average duration of the annotated bradycardias in s for the recording ($Duration_{WB}$),the number of the annotated bradycardias in the recording ($Number_{WB}$), the average RR amplitude during the bradycardia in ms (RR_{WB}), the sampling frequency of the ECG used to derive the tachogram in Hz ($F_{S,ECG}$), postmenstrual age in weeks (PMA) and gestational age in weeks (GA). The last three rows represent the number of recording for each age subgroups (below 32 PMA weeks, between 32 and 36 weeks and above 36 weeks). Blank spaces indicates that bradycardias were not annotated according to the definition in Section 2.2.

PAT_{ID}	REC_{ID}	$Duration_{Rec}$	$Duration_{WB}$	$Number_{WB}$	RR_{WB}	$F_{S,ECG}$	PMA	GA
18	3	210.438				250	34.57	25
22	1	296.328	20.625	8	703	250	28.71	25.43
22	2	175.143	27.417	1	808	250	34.29	25.43
174	1	262.792	15.306	3	645	500	32.29	31.43
174	2	272.96	28.583	2	460	250	34.29	31.43
32	2	65.065				250	36	32
32	3	133.833				250	37.43	32
33	1	57.332	9.667	1	610	500	27.29	25.71
33	2	184.832	27.639	9	540	500	29	25.71
33	3	120.942	11.75	1	730	500	31.14	25.71
33	4	264.74	25.156	16	572	500	32.71	25.71
33	5	228.619	17.319	6	603	500	34.71	25.71
34	1	196.621	23.292	12	607	500	27.29	25.71
34	2	136.526	31.208	6	599	500	29	25.71
34	3	128.192	11.833	1	633	500	31	25.71
34	4	251.589	22.893	7	598	500	32.71	25.71
34	5	146.753	18.463	9	590	500	34.71	25.71
34	6	539.988	19.683	10	666	250	40	25.71
35	2	221.486	6.667	1	771	250	34.14	30.43
35	3	251.707	6.583	1	631	250	35.71	30.43
35	4	446.989				250	36.57	30.43
37	1	243.658	23.515	11	612	500	31	30.29
37	2	223.356	14.048	21	630	500	33	30.29
37	3	577.278	29.842	61	524	250	36.71	30.29
38	1	258.396	18.25	5	814	500	31	30.29
38	2	251.453	4.667	2	664	500	33	30.29
38	3	565.986	27.258	59	564	250	36.71	30.29
40	1	100.2				250	31.43	30.29
40	2	495.688				250	36	30.29
44	1	303.978	14.033	5	606	500	29.57	24.57
44	2	195.789	13.1	5	607	500	31.57	24.57
44	3	146.025	21.083	1	577	500	34.57	24.57
44	4	81.593				500	37.71	24.57
60	2	213.171				500	34	31.89
60	3	472.993	5.083	1	592	250	36.29	31.89

Table S2. Continuation of Table S1.

PAT_{ID}	REC_{ID}	$Duration_{Rec}$	$Duration_{WB}$	$Number_{WB}$	RR_{WB})	$F_{S,ECG}$	PMA	GA
72	1	149.482	24.292	6	728	500	30.71	30
72	2	234.721	12.167	4	624	500	32.29	30
72	3	54.044				500	34	30
72	4	138.394				500	36	30
72	5	379.979	6.75	1	747	500	37.43	30
75	1	213.293	25.15	5	599	500	31.29	28.86
75	2	149.963				500	33.29	28.86
106	1	272.81	18.021	4	619	500	31.71	26.29
106	2	211.19	29.444	3	560	500	33.57	26.29
106	3	103.571				250	36.71	26.2857
79	1	271.892				500	30.29	29.86
79	2	130.792				500	33.71	29.86
79	4	129.625				500	36.71	29.86
79	5	137.285				500	40.57	29.86
88	2	175.725	24.722	3	716	500	30.43	26.71
88	3	236.161	18.604	12	613	500	32.14	26.71
88	4	60.208				500	35.29	26.71
88	5	142.931				500	37.14	26.71
90	1	241.475	14.833	4	564	500	28.71	25.29
90	2	184.988	22.6	5	615	500	30.43	25.29
90	4	68.238				500	34.57	25.29
90	5	184.693				500	38.57	25.29
159	1	255.615				500	32.57	29.57
159	2	209.44	13.317	5	763	500	34.43	29.57
159	3	98.794				500	36.57	29.57
160	1	165				500	32.71	29.57
160	2	92.985				500	36.71	29.57
160	3	170.431	11.583	3	788	500	40.86	29.57
171	1	125.431				500	32.14	29.29
171	2	88.658	32.833	4	514	500	33.71	29.29
171	3	217.708				500	40.29	29.29
133	1	193.583	12	3	570	500	30.71	27.71
133	2	186.324	39.083	1	597	500	32.43	27.71
133	3	63.25	7.583	2	709	500	34.43	27.71
56	2	107.964	20.542	2	598	250	33.14	30.57
57	1	173.315				500	30.86	30.57
57	2	292.147	7.472	3	604	500	33.14	30.57
19	1	246.489	24.783	5	625	250	32	30
19	2	143.161	26.667	7	565	250	34.57	30

Table S3. The main temporal, spectral and fractal features are reported for the post-bradycardia periods. The results are reported as median(IQR). IQR stands for *interquartile range*. The fractal indices are reported for $f_s = 8\ Hz$. The symbol ρ stands for the Pearson correlation coefficient. The symbol ** represents a significant correlation with $p \leq 0.01$, and * is used for a significant correlation with $p \leq 0.05$. $^{n.s.}$ is used to indicate a non-significant correlation.

Median(IQR) - PMA weeks	≤ 32	$(32-36]$	> 36	$\rho(\%)$
Temporal features in the post-bradycardia (PB) group				
μ_{RR}	374.65(366.38-391.36)	377.07(364.33-393.69)	387.2(374.98-416.44)	0.39**
σ_{RR}	16.71(12.02-22.05)	25.5(21.65-31.1)	28.47(24.03-32.08)	0.49**
Spectral features in the post-bradycardia (PB) group				
$P(VLF)_{Welch}$	106.24(63.14-156.22)	250.27(180.65-408.05)	287.59(219.04-454.15)	0.38**
$P(VLF)_{SPWD}$	643.16(434.61-1029.4)	1787.69(1081.86-2475.95)	2013.8(1252.61-2653.49)	0.39**
$P(VLF)_{Wavelet}$	36.25(19.22-56.58)	82.2(46.77-119.8)	89.58(62.29-139.78)	0.34*
$P(LF)_{Welch}$	10.91(5.35-16.13)	28.98(13.41-48.24)	50.5(19.82-67.56)	0.63**
$P(LF)_{SPWD}$	70.65(29-94.04)	141.99(84.7-219.13)	450.23(119.78-574.82)	0.69**
$P(LF)_{Wavelet}$	2.14(0.96-3.68)	4.17(2.16-8.9)	17.74(4.94-25.51)	0.69**
$P(HF)_{Welch}$	7.85(3.88-9.53)	9.99(6.08-13.7)	11.84(9.28-24.15)	0.22$^{n.s.}$
$P(HF)_{SPWD}$	38.05(22.98-68.8)	76.75(42.2-106.64)	124.07(87.74-210.87)	0.39**
$P(HF)_{Wavelet}$	0.69(0.36-1.3)	1.61(0.67-2.28)	3.57(1.55-6.4)	0.61**
$\frac{VLF}{LF}_{Welch}$	12.22(7.92-24.59)	9.9(5.8-18.72)	5.45(4.72-8.03)	0.06$^{n.s.}$
$\frac{VLF}{LF}_{SPWD}$	10.76(7.7-13.27)	7.68(4.98-15.57)	4.5(3.11-4.82)	-0.08$^{n.s.}$
$\frac{VLF}{LF}_{Wavelet}$	20.17(12.68-34.29)	19.6(7.22-26.37)	6.98(4.53-10.08)	-0.36**
$\frac{LF}{HF}_{Welch}$	1.47(1.05-1.96)	2.33(1.54-3.36)	3.91(1.9-4.94)	0.56**
$\frac{LF}{HF}_{SPWD}$	1.38(1.14-1.79)	1.91(1.71-2.74)	3.2(1.46-3.81)	0.57**
$\frac{LF}{HF}_{wavelet}$	2.27(1.87-3.02)	3.2(2.76-3.75)	4.56(3.04-5.24)	0.48**
$\frac{LF}{LF+HF}_{Welch}$	59.45(48.87-65.64)	69.97(60.1-76.75)	79.55(65.51-83.17)	0.45**
$\frac{LF}{LF+HF}_{SPWD}$	57.89(53.12-63.96)	65.63(63.1-73.15)	76.13(59.34-79.22)	0.48**
$\frac{LF}{LF+HF}_{Wavelet}$	69.44(65.16-74.67)	76.18(73.35-78.44)	81.96(75.27-83.65)	0.37**
$\frac{LF}{LF+VLF}_{Welch}$	9.11(5.32-12.28)	9.17(5.2-15.27)	15.99(13.78-17.47)	0.48**
$\frac{LF}{LF+VLF}_{SPWD}$	9.14(7.5-11.74)	11.53(6.04-16.74)	19.79(17.18-21.91)	0.56**
$\frac{LF}{LF+VLF}_{Wavelet}$	5.38(3.45-8.7)	4.9(3.67-12.17)	14.06(11.77-18.09)	0.57**
Fractal features in the post-bradycardia (PB) group				
$H_{exp,[j_1,j_2=5,12]}$	0.61(0.52-0.7)	0.55(0.45-0.59)	0.5(0.44-0.56)	-0.47**
$C_{2,[j_1,j_2=5,12]}$	-0.2(-0.26 - -0.17)	-0.19(-0.21 - -0.13)	-0.14(-0.15 - -0.11)	0.45**
$H_{exp,[j_1,j_2=3,12]}$	0.67(0.6-0.71)	0.66(0.59-0.69)	0.62(0.58-0.65)	-0.33*
$C_{2,[j_1,j_2=3,12]}$	-0.14(-0.16 - -0.1)	-0.11(-0.14 - -0.08)	-0.09(-0.11 - -0.09)	0.2$^{n.s.}$

Table S4. The main temporal, spectral and fractal features are reported for the between-bradycardias (BB) periods. The results are reported as median(IQR). IQR stands for *interquartile range*. The fractal indices are reported for $f_s = 8\ Hz$. The symbol ρ stands for the Pearson correlation coefficient. The symbol ** represents a significant correlation with $p \leq 0.01$, and * is used for a significant correlation with $p \leq 0.05$. $^{n.s.}$ is used to indicate a non-significant correlation.

Temporal features in the between-bradycardias (BB) group				
Median(IQR) - PMA weeks	≤ 32	$(32-36]$	> 36	$\rho(\%)$
Fractal features in the three age groups				
μ_{RR}	370.51(359.96-388.36)	377.42(363.11-389.25)	394.93(370.01-427.45)	0.47**
σ_{RR}	13.89(10.97-18.49)	19.81(15.72-23.82)	29.1(21.99-30.66)	0.64**
Spectral features in the between-bradycardias (BB) group				
$P(VLF)_{Welch}$	68.99(46.83-128.31)	156.67(100.26-217.63)	320.47(184.27-388.76)	0.54**
$P(VLF)_{SPWD}$	358.71(321.19-673.85)	991.87(498.71-1346.25)	2332.8(901.57-2915.13)	0.58**
$P(VLF)_{Wavelet}$	19.23(16.42-40.32)	58.93(35.74-75.05)	108(55.74-147.03)	0.63**
$P(LF)_{Welch}$	8.27(3.78-13.34)	14.99(5.95-25.28)	35.69(26.87-49.37)	0.66**
$P(LF)_{SPWD}$	46.5(25.63-88.72)	106.67(56.24-154.71)	273.11(213.86-373.31)	0.73**
$P(LF)_{Wavelet}$	1.3(0.86-3.38)	4.23(1.93-6.28)	11.34(8.4-15)	0.71**
$P(HF)_{Welch}$	4.85(3.47-6.9)	5.2(4.06-8.12)	11.55(6.11-13.56)	$0.17^{n.s.}$
$P(HF)_{SPWD}$	24.07(19.35-49.89)	50.8(25.85-85.57)	103.73(63.59-129.27)	$0.24^{n.s.}$
$P(HF)_{Wavelet}$	0.45(0.36-1.06)	0.91(0.53-2.2)	2.79(2.09-4.65)	0.62**
$\frac{VLF}{LF}_{Welch}$	9.4(7.9-13.65)	9.22(5.58-18.69)	5.29(4.7-8.4)	$-0.2^{n.s.}$
$\frac{VLF}{LF}_{SPWD}$	7.86(6.19-10.78)	7.5(5.3-13.48)	4.02(3.45-6.87)	$-0.14^{n.s.}$
$\frac{VLF}{LF}_{Wavelet}$	13.42(10.75-19.77)	11.73(8.1-21.36)	7(6.17-10.44)	$-0.3^{n.s.}$
$\frac{LF}{HF}_{Welch}$	1.42(0.75-2.16)	2.19(1.8-3.09)	3.78(2.39-4.23)	0.57**
$\frac{LF}{HF}_{SPWD}$	1.45(0.98-1.6)	1.87(1.61-2.18)	2.8(1.61-3.25)	0.52**
$\frac{LF}{HF}_{Wavelet}$	2.32(1.8-2.84)	3.2(2.39-4.11)	3.67(2.47-4.6)	0.33*
$\frac{LF}{LF+HF}_{Welch}$	58.67(42.64-67.61)	68.69(64.25-75.48)	78.97(70.53-80.88)	0.56**
$\frac{LF}{LF+HF}_{SPWD}$	59.11(49.57-61.62)	65.19(61.76-68.51)	73.67(61.65-76.48)	0.47**
$\frac{LF}{LF+HF}_{Wavelet}$	69.86(64.13-73.93)	76.21(70.43-80.43)	78.39(71.21-82.13)	0.33*
$\frac{LF}{LF+VLF}_{Welch}$	9.71(6.91-11.29)	9.87(5.18-15.21)	16.08(10.77-17.58)	0.42**
$\frac{LF}{LF+VLF}_{SPWD}$	11.29(8.24-13.6)	11.67(6.91-15.29)	19.55(12.12-21.93)	0.44**
$\frac{LF}{LF+VLF}_{Wavelet}$	6.93(4.89-8.53)	7.9(4.63-11.05)	12.57(8.75-13.95)	0.48**
Fractal features in the between-bradycardias (BB) group				
$H_{exp,[j_1,j_2=5,12]}$	0.6(0.52-0.68)	0.54(0.5-0.59)	0.48(0.45-0.52)	-0.5**
$C_{2,[j_1,j_2=5,12]}$	-0.19(-0.23 - -0.14)	-0.17(-0.2 - -0.14)	-0.09(-0.12 - -0.08)	0.43**
$H_{exp,[j_1,j_2=3,12]}$	0.68(0.61-0.73)	0.65(0.6-0.67)	0.6(0.55-0.62)	-0.36*
$C_{2,[j_1,j_2=3,12]}$	-0.12(-0.15 - -0.1)	-0.12(-0.14 - -0.1)	-0.08(-0.09 - -0.05)	$0.23^{n.s.}$

Table S5. The main temporal, spectral and fractal features are reported for the within-bradycardia (WB) periods. The results are reported as median(IQR). IQR stands for *interquartile range*. The temporal and spectral indices are reported for $f_s = 6\ Hz$ and the fractal index is reported for $f_s = 8\ Hz$. The symbol ρ stands for the Pearson correlation coefficient. The symbol ** represents a significant correlation with $p \leq 0.01$, and * is used for a significant correlation with $p \leq 0.05$. $^{n.s.}$ is used to indicate a non-significant correlation.

Temporal features in the within-bradycardia (WB) group.				
Median(IQR) - PMA weeks	≤ 32	$(32-36]$	> 36	$\rho(\%)$
Fractal features in the three age groups				
μ_{RR}	384.9(369.62-398.91)	384.16(369.2-397.51)	389.12(377.65-425.8)	0.37**
σ_{RR}	38.31(32.22-44.62)	40.61(32.5-49.81)	35.89(28.43-40.74)	-0.04$^{n.s.}$
Spectral features in the the within-bradycardia (WB) group.				
$P(VLF)_{Welch}$	167.75(101.36-282.21)	312.85(213.81-435.07)	300.05(226.89-457.86)	0.28*
$P(VLF)_{SPWD}$	1109.26(838.07-1615.84)	2025.93(1381.79-3909.12)	2168.01(1229.65-3824.98)	0.31*
$P(VLF)_{Wavelet}$	82.66(46.46-169.3)	122.69(69.22-230.91)	128.03(77.63-164.54)	0.1$^{n.s.}$
$P(LF)_{Welch}$	13(6.4-18.71)	31.09(15.62-52.49)	49.95(20.66-73.54)	0.59**
$P(LF)_{SPWD}$	102.62(68.87-185.63)	216.65(136.5-351.6)	502.28(152.3-734.74)	0.65**
$P(LF)_{Wavelet}$	2.3(1.12-4.03)	4.68(2.8-9.86)	18.66(5.35-26.46)	0.69**
$P(HF)_{Welch}$	7.73(4.31-10.01)	10.63(7.49-14.56)	12.21(9.75-25.52)	0.19$^{n.s.}$
$P(HF)_{SPWD}$	78.85(56.13-117.78)	106.08(78.08-182.35)	148.54(118.65-225.94)	0.3*
$P(HF)_{Wavelet}$	0.6(0.4-1.34)	1.49(0.74-2.57)	3.75(1.58-6.34)	0.59**
$\frac{VLF}{LF}_{Welch}$	13.25(9.99-25.23)	9.86(5.99-19.16)	5.62(4.53-7.99)	0.01$^{n.s.}$
$\frac{VLF}{LF}_{SPWD}$	8.3(6.56-12.13)	8.85(4.78-12.81)	4.18(2.93-4.69)	-0.08$^{n.s.}$
$\frac{VLF}{LF}_{Wavelet}$	43.62(24.21-96.77)	30.2(10.15-56.67)	9.21(4.96-13.94)	-0.47**
$\frac{LF}{HF}_{Welch}$	1.59(1.2-2.07)	2.28(1.69-3.51)	3.86(1.85-4.99)	0.52**
$\frac{LF}{HF}_{SPWD}$	1.3(1.19-1.51)	1.8(1.48-2.26)	2.89(1.35-3.25)	0.57**
$\frac{LF}{HF}_{Wavelet}$	2.36(1.89-2.99)	3.23(2.95-3.84)	4.67(3.02-5.3)	0.48**
$\frac{LF}{LF+HF}_{Welch}$	61.12(53.47-66.49)	69.5(62.38-77.32)	79.32(64.9-83.31)	0.41**
$\frac{LF}{LF+HF}_{SPWD}$	56.49(54.27-60.15)	64.06(59.6-69.35)	74.27(57.44-76.58)	0.49**
$\frac{LF}{LF+HF}_{Wavelet}$	70.22(65.4-74.94)	76.37(73.75-78.74)	82.34(75.1-84.11)	0.37**
$\frac{LF}{LF+VLF}_{Welch}$	7.28(4.92-9.1)	9.2(4.99-14.83)	15.38(14.34-18.08)	0.55**
$\frac{LF}{LF+VLF}_{SPWD}$	10.86(8.03-13.38)	10.86(7.2-17.11)	19.63(18.13-23.51)	0.52**
$\frac{LF}{LF+VLF}_{Wavelet}$	2.57(1.13-3.97)	3.34(2.19-8.97)	10.96(6.69-16.78)	0.64**
Fractal features in the within-bradycardia (WB) group.				
$H_{exp,[j_1,j_2=5,12]}$	0.61(0.49-0.71)	0.55(0.43-0.62)	0.49(0.43-0.52)	-0.45**
$C_{2,[j_1,j_2=5,12]}$	-0.26(-0.3- -0.21)	-0.21(-0.24- -0.17)	-0.13(-0.18- -0.11)	0.54**
$H_{exp,[j_1,j_2=3,12]}$	0.66(0.62-0.71)	0.64(0.58-0.68)	0.61(0.58-0.62)	-0.36**
$C_{2,[j_1,j_2=3,12]}$	-0.15(-0.2- -0.12)	-0.14(-0.17- -0.11)	-0.11(-0.12- -0.09)	0.31*